



**Politecnico  
di Torino**

POLITECNICO DI TORINO

Master's Degree course in Communications and Computer Networks  
Engineering

Master's Degree Thesis

**Advanced mitigation techniques  
for band-limited channels applied  
to digital multi-subcarriers optical  
systems**

**Supervisor**  
prof. Andrea Carena

**Candidate**  
Clara SALVALAI  
matricola: 279936

A.y. 2021/2022



# Summary

The study and the analysis presented in this thesis consider a fiber-optic transmission system in which the signal is routed from the source to the destination using devices called Reconfigurable Optical Add-Drop Multiplexers (ROADMs). These devices act as multiplexers, being able to select a certain wavelength and route it to the local RX (Drop) or to choose new traffic to route from a TX (Add). They rely on Wavelength Selective Switches (WSS) that act like filters on the signal, impairing it on the frequencies at the edges.

In particular, the larger the number of cascaded WSS, the greater the impact on the signal. To mitigate the impact of filtering on transmission, a promising solution consists in dividing the channel into subcarriers, each with the same spectral bandwidth, and adopt advanced techniques able to limit the filtering impact. Moreover, the usage of multi-subcarriers (MSC) systems is also beneficial to adjust the data rate with finer granularity, which is becoming important in recent years since data traffic is more heterogeneous. This can be obtained by exploiting Frequency Domain Hybrid Modulation Formats (FDHMF), that allows to assign a different modulation format to each subcarriers.

In this thesis, standard single carrier transmission is compared to MSC systems. Specifically, two modulation format approaches, Uniform QAM Constellation and Probabilistic Constellation Shaping (PCS). With Uniform QAM Constellation, all the constellation symbols are equiprobable. With PCS, instead, constellation symbols are no longer equiprobable but rather distributed according to a probability distribution, meaning that the initial  $2^M$ -QAM constellation is "shaped" in order to operate closer to the fundamental Shannon Limit.

On top of this, further optimization strategies based on bit and/or power loading (in case of Uniform QAM Constellation) and on entropy loading with/without water-filling (in case of PCS) are studied to improve the system performance.

Applying the above mentioned techniques it was possible to optimize the transmission and see some advantages. It has been shown that, in general, the MSC approach performs better than the standard Single Carrier case when several WSS impair the signal and, additionally, that the PCS technique with its strategies outperforms the Uniform QAM Constellation.



# Acknowledgements

I would like to express my gratitude to the Supervisor of this thesis, professor Andrea Carena, for guiding me through the world of optical communications. It has been a fascinating journey.

A special thank to Doctor Ann Margareth Rosa Brusin for all the support she gave me over all these months.

Then, I would like to thank my father for always being by my side and for transmitting me his passion for scientific disciplines. Everything I achieved has been possible only thanks to him.

Thanks to Andrea, your support is vital.

Thanks to my old friends always able to donate lightheartedness.



# Contents

<b>List of Tables</b>	8
<b>List of Figures</b>	9
<b>1 Introduction</b>	13
1.1 Optical fiber networks . . . . .	13
1.2 Optical fiber link . . . . .	16
1.2.1 Optical fiber structure . . . . .	16
1.2.2 Optical Amplifiers . . . . .	18
1.3 Optical signal transceiver . . . . .	19
1.3.1 Coherent RX . . . . .	20
1.3.2 DSP Block Diagram . . . . .	21
1.3.3 PM-I/Q Modulator . . . . .	23
1.4 Digital Subcarrier Multiplexing . . . . .	24
1.5 Goal and organization of the thesis . . . . .	25
<b>2 Impact of WSS filtering: a theoretical analysis</b>	27
2.1 Current Scenario . . . . .	27
2.2 Uniform QAM Constellation . . . . .	29
2.3 Probabilistic Constellation Shaping . . . . .	31
2.3.1 Entropy Loading algorithm . . . . .	36
<b>3 Simulation Results</b>	39
3.1 BER and MI . . . . .	40
3.2 Uniform QAM Constellation Comparison . . . . .	43
3.3 PCS Comparison . . . . .	50
3.4 Uniform QAM Constellation and PCS Comparison . . . . .	63
<b>4 Conclusions</b>	67
<b>Bibliography</b>	69

# List of Tables

2.1	Hybrid Bit Loading combinations. . . . .	31
3.1	Power Ratio values applied per subcarriers using the Power Loading Technique, starting from SNR = 20 dB and SNR = 25 dB. . . . .	49
3.2	Constellation order per subcarrier chosen by Bit Loading technique.	49
3.3	Constellation order per subcarrier chosen by Bit and Power Loading technique in a system using 16 subcarriers. . . . .	50
3.4	$R_b$ and $MI_{target}$ values for different $\lambda$ . . . . .	53
3.5	Shaping factor $\lambda$ optimized for all subcarriers for different number of cascaded WSS using EL and WF techniques. . . . .	58
3.6	Power Ratio for different SNR values using Waterfilling technique. .	59

# List of Figures

1.1	Scheme of a point to point communication system . . . . .	14
1.2	Logical scheme of a WSS. Credits: from slides of the Seminar on Software-defined Optical Networks, Prof. Vittorio Curri, Politecnico di Torino. . . . .	14
1.3	Scheme of a ROADMs. Credits: from slides of the Seminar on Software-defined Optical Networks, Prof. Vittorio Curri, Politecnico di Torino. . . . .	15
1.4	Optical Network scheme with nodes crossed by lighpaths, from slides of the Seminar on Software-defined Optical Networks, Prof. Vittorio Curri, Politecnico di Torino. . . . .	15
1.5	Structure of a fiber used for optical transmission. Credits: from slides of "Devices for Optical and Microwave Communications" course, Prof. Guido Perrone, Politecnico di Torino. . . . .	16
1.6	Levels of refractive index for cladding and core. Credits: from slides of "Devices for Optical and Microwave Communications" course, Prof. Guido Perrone, Politecnico di Torino. . . . .	17
1.7	Fiber attenuation as a function of wavelength. . . . .	18
1.8	Scheme of a multi-span fiber. Credits: from slides of "Optical and Wireless Communications" course, Prof. Roberto Gaudino, Politecnico di Torino. . . . .	18
1.9	Example of PAM-2, PAM-4 and PAM-8 . . . . .	19
1.10	Scheme of the coherent RX. Credits: from slides of "Optical and Wireless Communications" course, Prof. Roberto Gaudino, Politecnico di Torino. . . . .	20
1.11	DSP Block Diagram . . . . .	21
1.12	Example of PM-QPSK modulation. Credits: from slides of "Optical and Wireless Communications" course, Prof. Roberto Gaudino, Politecnico di Torino. . . . .	23
1.13	Scheme of an I/Q Modulator considering just the $\hat{y}$ polarization. Credits: from slides of "Optical and Wireless Communications" course, Prof. Roberto Gaudino, Politecnico di Torino. . . . .	24

1.14	Example of Power Spectrum for the Single Carrier and MSC cases. Credits: [2]. . . . .	25
2.1	Transfer functions of cascaded WSS for $N_{WSS} \in \{0, \dots, 10\}$ units given by expression 2.1, where $B = 134.375$ GHz and $BW_{OTF} = 10.4$ GHz. . . . .	28
2.2	Example of filtering effects on a 128 GBaud single-carrier signal due to 10 cascaded WSSs . . . . .	29
2.3	Example of filtering effects on a 128 GBaud multi-subcarrier signal due to 10 cascaded WSSs . . . . .	29
2.4	Bit Rate curves. . . . .	33
2.5	$\lambda$ vs $R_b$ . . . . .	33
2.6	Probability density functions of PCS constellations for different shap- ing levels. . . . .	34
2.7	Scatter plot of the constellation point at the Rx. . . . .	35
2.8	Power redistribution according to the Water Filling technique . . . . .	36
2.9	Look Up Table storing the relations between NGMI, SNR and H. . . . .	37
3.1	BER values for a transmission with 8 subcarriers and without filters . . . . .	40
3.2	MI values for a transmission with 8 subcarriers and without filters . . . . .	40
3.3	Required SNR obtained from both BER and MI. . . . .	41
3.4	Comparison of BER theory and BER simulated, without filters. . . . .	42
3.5	Comparison of BER theory and BER simulated, with 5 filters. . . . .	42
3.6	Comparison of BER theory and BER simulated, with 10 filters. . . . .	42
3.7	Comparison between theoretical and simulated required SNR. . . . .	42
3.8	BER values for a transmission with 8 subcarriers and filters nWSS $\in \{0, \dots, 10\}$ . . . . .	43
3.9	MI values for a transmission with 8 subcarriers and filters nWSS $\in$ $\{0, \dots, 10\}$ . . . . .	43
3.10	Comparison of techniques using 16-QAM with nSC = 8, 16, 32, 64. . . . .	44
3.11	Comparison of techniques using 64-QAM with nSC = 8, 16, 32, 64. . . . .	45
3.12	Bit Loading and Bit and Power Loading applied up to 16 WSSs for different nSC and M-QAM. . . . .	46
3.13	Comparison of nSC for 16-QAM applying Same Power. . . . .	47
3.14	Comparison of nSC for 16-QAM applying Power Loading. . . . .	47
3.15	Comparison of nSC for 16-QAM applying Bit Loading. . . . .	47
3.16	Comparison of nSC for 16-QAM applying Bit and Power Loading. . . . .	47

3.17 Comparison of nSC for 64-QAM applying Same Power. . . . .	48
3.18 Comparison of nSC for 64-QAM applying Power Loading. . . . .	48
3.19 Comparison of nSC for 64-QAM applying Bit Loading. . . . .	48
3.20 Comparison of nSC for 64-QAM applying Bit and Power Loading. . . . .	48
3.21 MI comparison without filters, 800 G. . . . .	51
3.22 MI comparison with 10 filters, 800 G. . . . .	51
3.23 MI comparison without filters, 1.2 T. . . . .	51
3.24 MI comparison with 10 filters, 1.2 T. . . . .	51
3.25 Probabilistic Constellation Shaping used in Single Carrier systems. . . . .	52
3.26 MI and $MI_{target}$ variation with respect to $\lambda$ . . . . .	53
3.27 3-D plot showing how the MI value depends on both SNR and $\lambda$ . . . . .	54
3.28 Required SNR vs $\lambda$ with nWSS $\in \{0..5\}$ , for both Single Carrier and 8 subcarriers cases. . . . .	54
3.29 Required SNR vs $R_b$ with nWSS $\in \{0..5\}$ , for both Single Carrier and 8 subcarriers cases. . . . .	55
3.30 Comparison of MI values obtained through theory and simulation in different conditions. . . . .	56
3.31 Comparison between theory and time-domain simulation for Entropy Loading with nSC = 8, 16, 32, 64. . . . .	57
3.32 MI versus SNR obtained for vectors of shaping factors optimized for different levels of SNR. . . . .	58
3.33 Comparison between Entropy Loading with and without Waterfilling in the 800G system for different number of subcarriers. . . . .	60
3.34 800G PCS applied with nSC = 8, 16, 32, 64. PCS + SP stands for PCS using the Same Power strategy, PCS + EL & WF for PCS using both the Entropy Loading and Waterfilling strategies. . . . .	61
3.35 1.2T PCS applied with nSC = 8, 16, 32, 64. PCS + SP stands for PCS using the Same Power strategy, PCS + EL & WF for PCS using both the Entropy Loading and Waterfilling strategies. . . . .	62
3.36 800G and 1.2T Entropy Loading for different nSC. . . . .	63
3.37 Uniform QAM Constellation and PCS final comparison for 800G. . . . .	64
3.38 Uniform QAM Constellation and PCS final comparison for 1.2T. . . . .	65
3.39 Single Carrier comparison for 800G and 1.2T. . . . .	66



# Chapter 1

## Introduction

### 1.1 Optical fiber networks

Today, voice, data and video transmission services are distributed through a public telecommunications network, which is made up mostly of optical fiber. The structure of the optical public telecommunications network can be differentiated according to its length into:

1. *Access Network*, connects the end user to the nearest central office, only a few kilometers long;
2. *Metropolitan Network*, connects nearby central offices to each other, about a few tens of kilometers long;
3. *Long Haul Core Network*, connects countries and continents even through submarine networks, thousands of kilometers long.

The use of optical fiber in public transportation networks is widely diffused nowadays, to the extent that it has become the reference technology used when high bandwidth and low distance are required in a communication system. The most simple topology of a transmission system based on optical fiber is the point-to-point scheme that, similar to other telecom systems, is made of: a transmitter (TX), a receiver (RX), and the optical fiber connecting the two as shown in Fig. 1.1.

In optical transmissions, the best way to route the signal from the TX to the RX is by using so-called transparent networks. A network is defined as "transparent" if the signal remains in the optical domain throughout the network. A transparent network is considered attractive due to its flexibility and higher data rate. Electronic components, in fact, would create a bottleneck for transmission speed and cause large power consumption. In transparent networks, the signal is routed from source to destination through a series of nodes using devices called Reconfigurable Optical Add/Drop Multiplexers (ROADMs), crucial to provide flexibility and reconfigurability to the optical transport network. A ROADM node is an array of



Figure 1.1. Scheme of a point to point communication system

Wavelength Selectable Switches (WSSs), devices with 1 optical input and  $N$  optical outputs able to convey a spectral slice (not necessarily exactly one channel) from the input to the selected output (Fig. 1.2). All the traffic passing through a

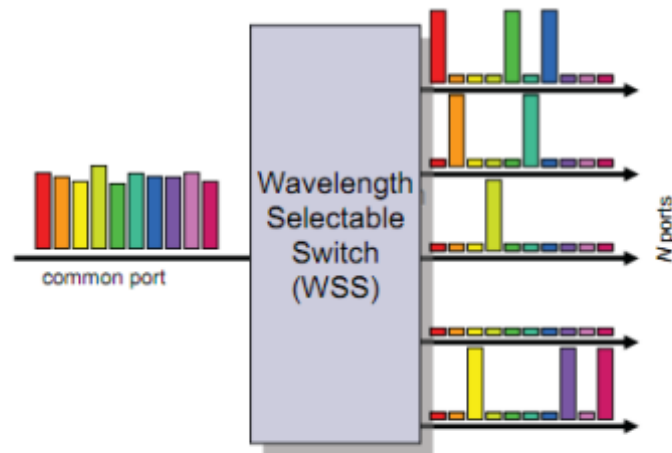


Figure 1.2. Logical scheme of a WSS. Credits: from slides of the Seminar on Software-defined Optical Networks, Prof. Vittorio Curri, Politecnico di Torino.

ROADMs can be divided into (Fig. 1.3):

1. *Express Traffic*, the one that is transparently routed across the device;
2. *Dropped Traffic*, the set of wavelengths dropped from the optical infrastructure to be received by a local transceiver;
3. *Added Traffic*, opposite the dropped, is the traffic joining the express traffic from the local node.

Switching matrices for ROADMs can be reconfigured dynamically, so the network becomes an elastic set of possible lightpaths called routing space, an example scheme

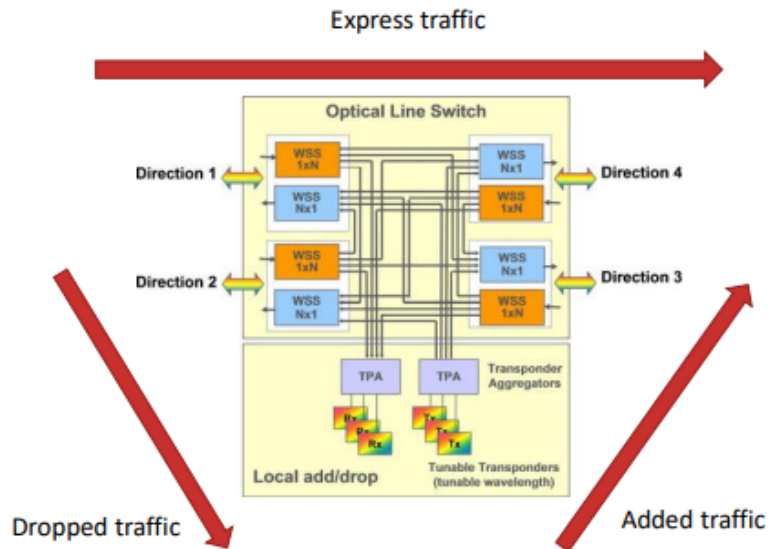


Figure 1.3. Scheme of a ROADMs. Credits: from slides of the Seminar on Software-defined Optical Networks, Prof. Vittorio Curri, Politecnico di Torino.

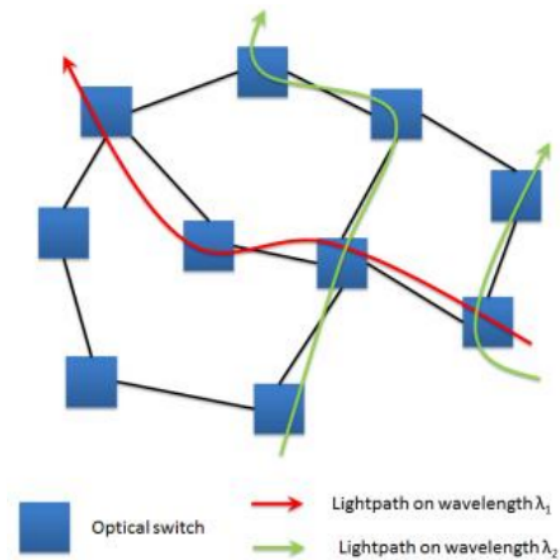


Figure 1.4. Optical Network scheme with nodes crossed by lightpaths, from slides of the Seminar on Software-defined Optical Networks, Prof. Vittorio Curri, Politecnico di Torino.

can be seen in figure 1.4. However, these devices have also some drawbacks, in fact, they bring other possible impairments to the signal passing through them such as Gaussian noise introduced by amplifying stages, interference from side channels, or filtering effects induced by the WSS transfer function on the channel, whose analysis is the focus of this thesis.

## 1.2 Optical fiber link

Nowadays, optical networks need to be built in such a way that they can connect long distances, over 100 km. To be able to reach such distances, optical fiber alone is not sufficient, there is the need of amplifiers capable of periodically expanding the signal, which would otherwise be ruined by losses and noise. The components of an optical link, fiber and amplifiers, will now be separately analyzed.

### 1.2.1 Optical fiber structure

Optical fibers used in telecommunication systems are usually made of highly purified silica glass ( $SiO_2$ ) and their structure can be divided into three concentric parts (Fig. 1.5):

1. the *core* is the inner part;
2. the *cladding* surrounds the core;
3. the *coating*, the outer section, can be divided into several layers protecting the Core and Cladding from the environment, it is made of plastic;

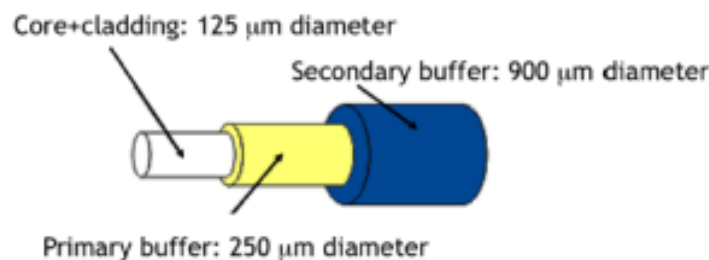


Figure 1.5. Structure of a fiber used for optical transmission. Credits: from slides of "Devices for Optical and Microwave Communications" course, Prof. Guido Perrone, Politecnico di Torino.

The main characteristic of the optical fiber is its ability to guide light within the core without scattering it along the way. This is allowed by a proper choice of the material with which the silica glass of Core and Cladding is doped. More specifically, the core should have a larger refractive index than the cladding (Fig. 1.6) and this is provided by doping the silica with Germanium to increase the index or with Fluorine to reduce it. The previous condition ensures the electromagnetic field to remain confined in the core of the fiber.

Moreover, it is possible to distinguish also between Single Mode (SMF) and Multi-

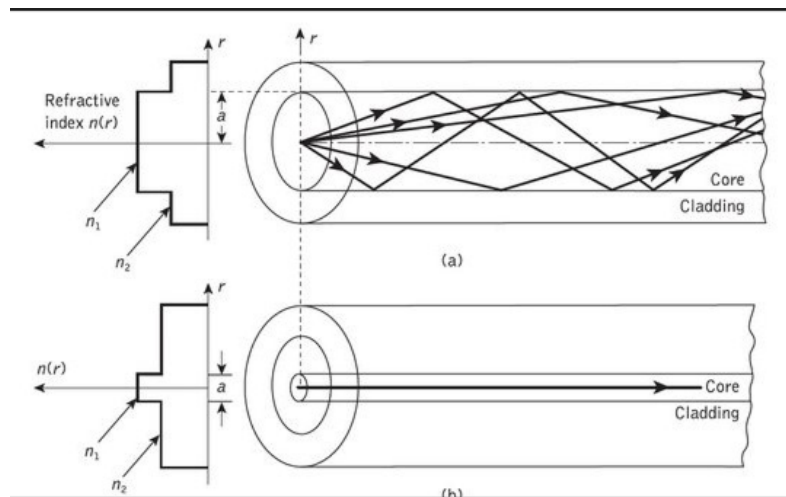


Figure 1.6. Levels of refractive index for cladding and core. Credits: from slides of "Devices for Optical and Microwave Communications" course, Prof. Guido Perrone, Politecnico di Torino.

Mode (MMF) fibers where a “mode” in a fiber is the path taken by the light. These two typologies have different characteristics, first of all the core diameter: for SMFs the core is generally  $10 \mu\text{m}$  wide while for MMFs it is wider, in the range from  $50$  to  $100 \mu\text{m}$ . In contrast, the cladding diameter remains  $125 \mu\text{m}$  for both types. In SMF just one path is allowed, producing low *dispersion* and small *attenuations*, both very advantageous especially for long-haul communication systems.

*Dispersion* is the spreading of the signal over time, it is generally divided into Chromatic or Modal, since we are focusing on single-mode let’s just focus on the first one. Chromatic dispersion is the most important linear distortion effect, the consequence of the unequal speed at which different frequencies can travel. It becomes more relevant by increasing bit rate and/or distance.

Instead, by *Attenuation* we mean the power reduction of the input signal transmitted along the fiber. It occurs in both multi-mode and single mode transmission but is exceptionally low for fibers compared to all other transmission media. In fact, in the typical frequency range used for fiber-optic transmissions (the so-called C-band, from  $191$  to  $196 \text{ THz}$ ), the attenuation is about  $0.2 \text{ dB/km}$ . However, after

hundreds or thousands of kilometers, it becomes a significant loss. From Fig. 1.7 we can see that, besides the C-band, other bands can be used but the lowest attenuation occurs exactly at a wavelength of 1550 nm, just in the middle of the C-band. However, there is one more advantage in operating within the C-band it is the frequency range where the best and the cheapest optical amplifiers can be built. This coincidence is accidental since the physical phenomena are unrelated.

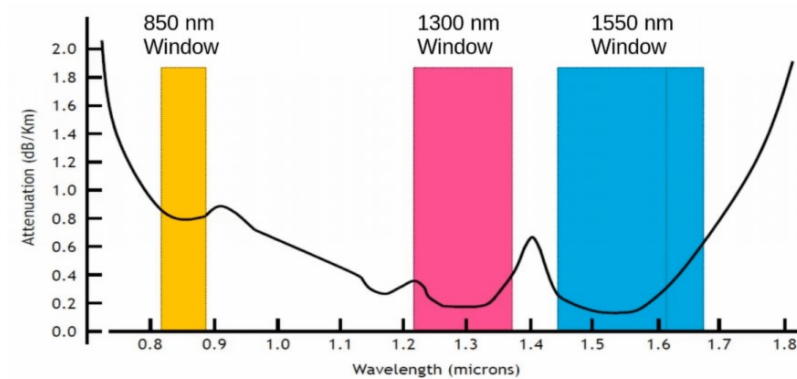


Figure 1.7. Fiber attenuation as a function of wavelength.

## 1.2.2 Optical Amplifiers

Erbium Doped Fiber Amplifiers, EDFA, are devices that can amplify an optical signal without any conversion to the electric domain through a physical operation called *Stimulated emission*. The advantage of having a cheap and reliable amplifier is the possibility of creating a long-haul optical link made of segments, called *spans*, each of them composed of a piece of fiber and an EDFA (Fig. 1.8).

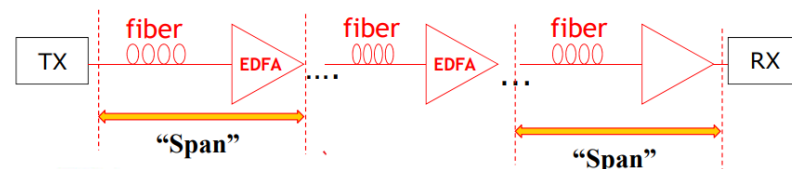


Figure 1.8. Scheme of a multi-span fiber. Credits: from slides of "Optical and Wireless Communications" course, Prof. Roberto Gaudino, Politecnico di Torino.

## 1.3 Optical signal transceiver

Another key aspect that characterizes one type of optical link from another is the way the optical power is converted into electrical current at the receiver. The so-called, detection can be distinguished between Direct Detection (DD) and Coherent Detection, which are performed using two different receivers.

*Direct Detection* is simpler and cheaper and typically it is used when intensity modulation (IM) is performed at the transmitter side to encode the digital information. More precisely, IM is based on the instantaneous variation of the optical power. Because of that, the only type of modulation allowed, at the transmitter, is Pulse Amplitude Modulation, PAM-M. Examples of typical PAM-M modulations are shown in Fig. 1.9.

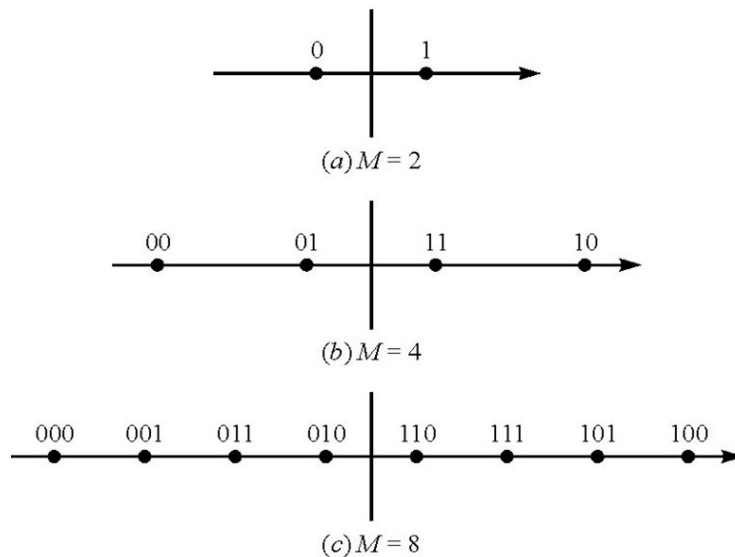


Figure 1.9. Example of PAM-2, PAM-4 and PAM-8

DDs receivers are often used together with the Mach-Zehnder modulator that allows generating a pure signal without a chirp. The receiver key element is a photodiode, in charge of converting the input optical power into an output electrical current. Intensity Modulation and Direct Detection (IM-DD) systems are, for example, used in Data Centers among servers or in Passive Optical Networks (PON) for local access (FTTH).

*Coherent Detection* systems are more recent than DD and they were introduced in order to reach much higher bit rates. This is possible since the Coherent receiver allows us to detect the information coming also from phase and polarization components, exploiting all the 4 degrees of freedom available in the optical fiber. Thus, the electrical field can be expressed as in Eq. 1.1.

$$E(t) = [E_{Rx}(t) + jE_{Ix}(t)]\hat{x} + [E_{Ry}(t) + jE_{Iy}(t)]\hat{y} \quad (1.1)$$

Where  $E_{Rx}(t)$  and  $E_{Ix}(t)$  are the real and imaginary components of the x-polarization, while  $E_{Ry}(t)$  and  $E_{Iy}(t)$  are, symmetrically, the real and imaginary components of the y-polarization.

### 1.3.1 Coherent RX

A schematic representation of the Coherent RX can be found in figure 1.10. From the figure it can be noticed that two different signals are considered:  $E_{ph}$  is the received optical signal,  $E_{LO}$  is called "Local Oscillator" and it is the reference signal used by the receiver to divide the In-phase and Quadrature components. Both those signals enter the Polarization Beam Splitter (PBS) block, able to split the two x and y polarizations. Then, for each polarization the two signals pass through the block called in the figure "Special Optical Device", known as "90° Hybrid" which creates four copies of the LO, that are 90 degrees off-phase, and it adds and subtracts them to the signal. So two signals enter the 90° hybrid and four exit. Finally, those signals are passed to the Balanced Photo-Detector (BPD), able to eliminate some unwanted power components coming from the previous block. The four extracted components are orthogonal to each other, but they can be misaligned with the reference axes at TX. So, as the receiver extracts the four orthogonal components, through electrical Digital Signal Processing (DSP) it is possible to “re-align” the reference axes to the transmitted ones, and decode the signal correctly. It can be concluded that the coherent receiver requires the DSP use.

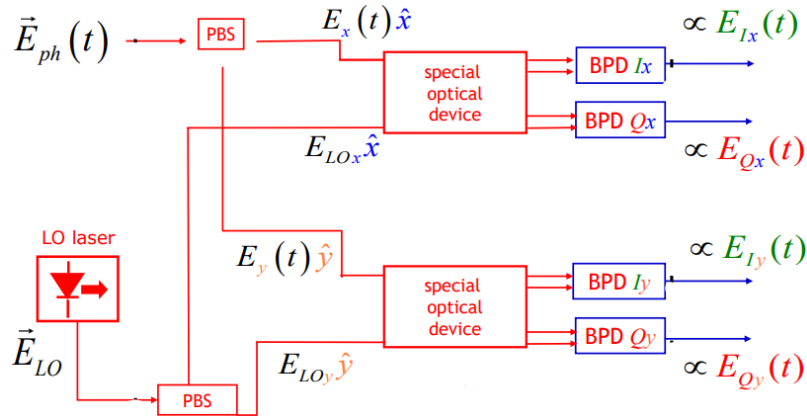


Figure 1.10. Scheme of the coherent RX. Credits: from slides of "Optical and Wireless Communications" course, Prof. Roberto Gaudino, Politecnico di Torino.

### 1.3.2 DSP Block Diagram

Fig. 1.11 shows the block diagram of the DSP available within the OptDSP library that has been used for our analyses. First of all, a digital signal processor, DPS, is a microprocessor that specializes in the operations required in the field of digital signal transmissions, such as in telecommunications, audio signal processing, or digital image processing. It is capable of performing a large number of mathematical and logical operations on a real-time data set and can rely on memory architectures capable of fetching multiple instructions at a time. The diagram starts from

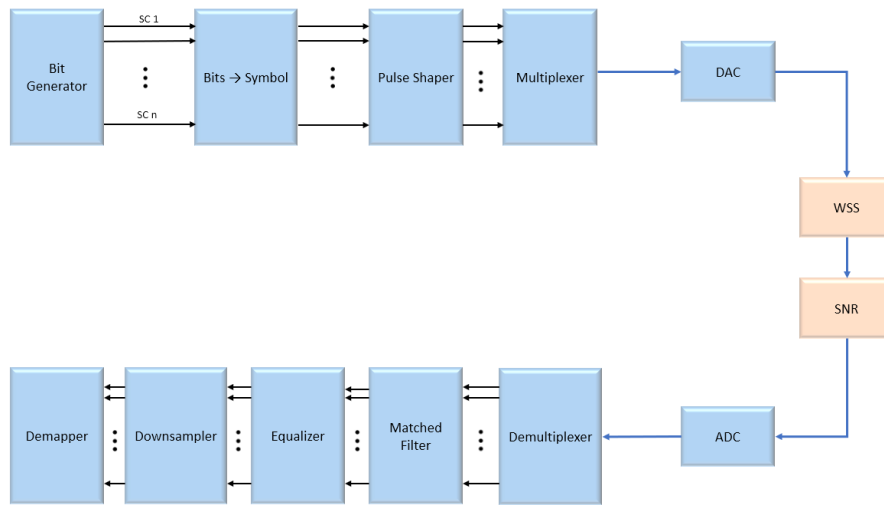


Figure 1.11. DSP Block Diagram

the transmitter, which performs various operations to build the signal; the first is the *bit generation block* which takes in input: the number of symbols that have to be generated  $Syms$ , the constellation order  $M$ , the number of polarizations, which in our case are always two, and finally the bit source telling how to generate the bits. The generated sequences are Pseudo-Random Binary Sequence, PRBS, which means that are a series of 1's and 0's random within the sequence length, it is considered a “worst case” stress test since there is no correlation between adjacent bits; despite the sequence is internally random, the way it is generated is deterministic since it is based on a seed, this implies that the sequence will always be the same when repeated allowing for mutually comparable tests [12]. This block returns as output two bit's strings, one per polarization, for each subcarrier.

The subsequent block translates the *bits into the corresponding symbols*. If the translation is done considering Uniform QAM Constellation, the order of the constellation  $M$  is used to know the number of bits per symbol,  $\log_2(M)$ , and thus the number of symbols to be generated. Then the stream of bits is associated with that of the corresponding symbol indices, and finally the indices are paired with

the constellation points on the I-Q plane, thus creating the actual complex signal to be transmitted.

The *Pulse-Shaper block* applies a pulse shaping filter with the intent to create signals, one per SC, that are band-limited, and reduce ISI. In our simulations, the filter is the Root Raised Cosine, defined by the equation 1.2.

$$h_{RRC} = \frac{\left[ \frac{4\rho}{\pi} \cos\left(\frac{(1+\rho)n\pi}{R}\right) \right] + \left[ (1-\rho) \operatorname{sinc}\left(\frac{(1-\rho)n\pi}{R}\right) \right]}{\sqrt{R} \left[ 1 - \left(\frac{4\rho n}{R}\right)^2 \right]} \quad (1.2)$$

Where  $\rho$  is the rolloff factor, which determines the slope of the filter, in our case  $\rho = 0.05$ , and  $R$  is the number of samples per symbol [13]; the output of this block are nSC shaped complex signals.

We proceed with the *multiplexing block*, in which the input signals generated for each subcarrier are combined together to form a single MSC signal.

The last transmitter block is the *DAC*, Digital to Analog Converter, it is necessary because in a fiber optic communication system, transmission occurs through a physical medium, so, after setting the information digitally, a transformation to the analogical form is necessary.

At this point the cascade of *WSS filters* will be applied to the transmitted signal; which provide the effect already described of attenuating the external subcarriers and degrading the information carried by them.

In the next block, the channel noise is applied and the *SNR is set*; noise is generated in a pseudo-random way with a fixed seed to guarantee the same noise insertion between different runs of the simulation. The last two blocks are not necessarily separated, in fact this is just the 'lumped' configuration, the one used in the coming simulations. This corresponds to a worst case scenario, since the noise is added all together at the end of the transmission, and it is not filtered by the cascaded WSS. The second one, on the other hand, represents a more realistic scenario, in which the noise is inserted as we go along the channel and thus also passes through the filters, undergoing attenuation.

After transmission, the signal is converted back to digital by the *ADC* block, Analog to Digital Converter, so that it can be decoded by the receiver. The digital signal will then retrace approximately the transmitter steps back, first entering the *demultiplexer block*, which, with shifts in frequency opposite to those of the MUX is able to split the nSC signals.

The next block is that of the *matched filter*, so called because it must "match" the input signal pulse, which in this case is shaped by the RRC filter in the transmitter, in order to maximize SNR in the presence of Additive White Gaussian Noise (AWGN).

The signals then pass through the *MIMO Adaptive Equalizer*, where MIMO stands for Multiple-Input Multiple-Output since it takes nSC input signals and returns

nSC output signals. The equalizer is responsible for compensating for signal damage due to the frequency response of the channel, which affects both amplitude and phase. Their operation is based on algorithms that derive coefficients used to recreate the impact of the channel that is then applied to the signal with opposite sign, so as to cancel them out. It is called Adaptive because the coefficients change to, precisely, adapt to channel impairments and so at the beginning of the transmission they need a training frequency to be adjusted.

The signal is then *downsampled* from 2 samples/symbol to 1 sample/symbol, this reduces the resolution of the signal but halves the number of symbols that then have to be decoded in the next and final step, speeding up the receiving process.

Finally, the signals enter the *demapper block* where they are first converted into the corresponding symbols of the constellation by taking advantage of the minimum distance detection between the received symbols and those of the source constellation, and later they are translated into bits. This process is performed both on the received signal, thus the one deteriorated by filters and channel noise, and on the transmitted signal, which will serve as a comparison for BER and MI calculations in order to understand how reliable the transmission was.

### 1.3.3 PM-I/Q Modulator

As a consequence of the possibility of exploiting the 4 degrees of freedom, at the TX side, the modulator has to be more complex and expensive in order to apply polarization multiplexing (PM) to both the in-phase (I) and the quadrature (Q) components, which are the real and the imaginary parts of the signal, respectively. An example is presented in Fig. 1.12. The corresponding modulator is called the

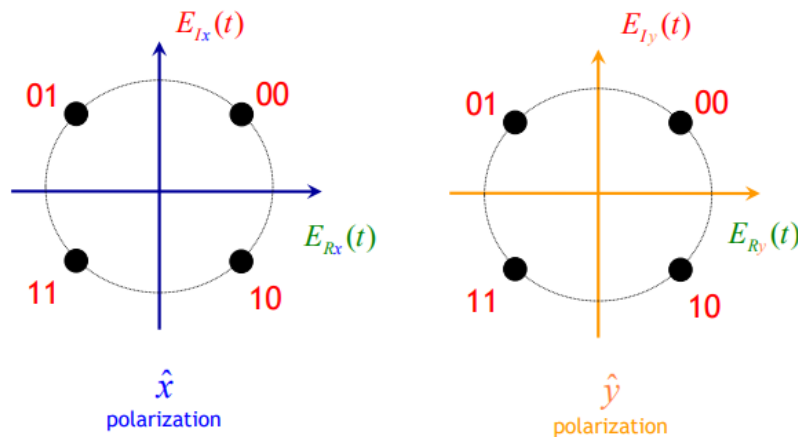


Figure 1.12. Example of PM-QPSK modulation. Credits: from slides of "Optical and Wireless Communications" course, Prof. Roberto Gaudino, Politecnico di Torino.

PM-I/Q modulator and it is composed by two I/Q modulators connected to a BPS to combine the two  $\hat{x}$  and  $\hat{y}$  polarizations. The I/Q modulator scheme is reported in figure 1.13. Each of the two I and Q signal is modulated with a Mach-Zehnder modulator, then the imaginary signal is shifted 90 degrees out of phase and is summed with the real one.

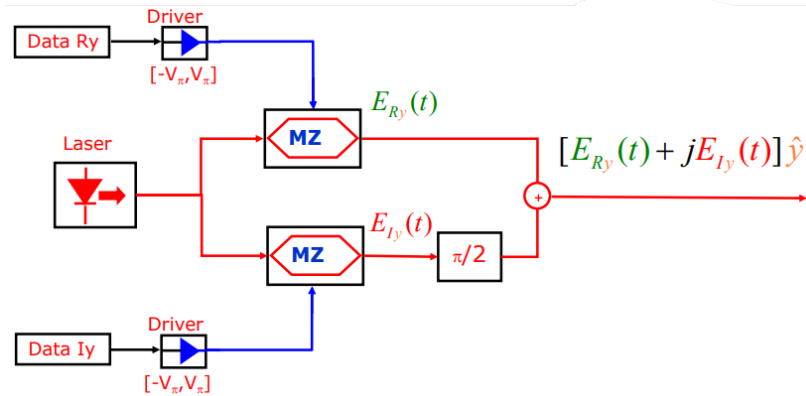


Figure 1.13. Scheme of an I/Q Modulator considering just the  $\hat{y}$  polarization. Credits: from slides of "Optical and Wireless Communications" course, Prof. Roberto Gaudino, Politecnico di Torino.

Long-haul fiber systems are nowadays based on the coherent technology, and indeed in this thesis, PM-I/Q modulation has been used to simulate a realistic transmission.

## 1.4 Digital Subcarrier Multiplexing

A main topic of this thesis is the Digital Subcarrier Multiplexing, a technique able to split the high-baud-rate Single Carrier signal into multiple low-baud-rate subcarriers. The realization of this feature was made just thanks to the development of high-speed digital-to-analog converters (DAC) and through the employment of the DSP device not only at RX, where is mandatory, but also at TX. For example, giving a 128 GBaud total Baud rate, if the signal is split into 2 subcarriers each of them will have 64 GBaud of Baud rate, if it is split in 4 the Baud rate will be 32GBaud, and so on. In figure 1.14 a graphical representation of a frequency channel divided in subcarriers is presented. Digital subcarrier multiplexing is considered an efficient candidate for fiber nonlinearity mitigation. The Multi-subcarrier (MSC) approach, in this work, will be always compared with the correspondent Single Carrier. The number of used subcarriers will be changed in order to understand which is the optimum configuration.

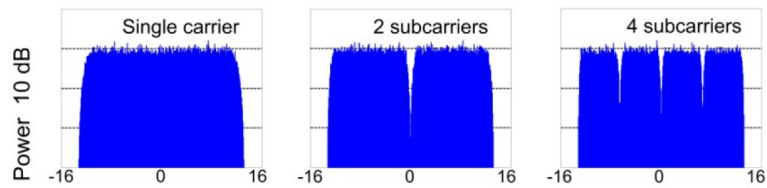


Figure 1.14. Example of Power Spectrum for the Single Carrier and MSC cases. Credits: [2].

The MSC approach, in the following analysis, is exploited applying techniques that can be distinguished into two major categories: Uniform QAM Constellation  $2^M$ -QAM, where  $M$  is the constellation cardinality, and Probabilistic Constellation Shaping (PCS). What differentiates the two techniques is the probability assigned to each constellation symbol. For Uniform QAM constellations the probability is uniformly distributed, all symbols have the same probability of being transmitted. In PCS, on the other hand, the probability follows a Gaussian-like distribution, further explained in Chapter 2. As a consequence the symbols in the center of the constellation, may have a higher probability of being transmitted than the outer ones. PCS is a more advanced technique than Uniform QAM Constellation, it has been taken into consideration since it is able to provide a finer bit-rate granularity and better results than the other. The advantages will be illustrated in more details in the following chapters.

To implement the PCS technique, an additional block must be inserted in the DSP block diagram presented in figure 1.11, the Distribution Matcher (DM). This block performs a fixed-length invertible mapping from an independent and uniformly distributed input bits into a sequence of output symbols with a desired distribution.

## 1.5 Goal and organization of the thesis

To cope with today's increase in Internet traffic demanded by services such as high-quality video, optical communications systems have been dominated by increasingly high cardinality modulations on a single carrier. It is well known that in order to meet these new challenges it is necessary to have a system that can both carry information at high bit rates and adapt its channel capacity in flexible manners and with fine granularity [1]. In a modern optical network, the signal is routed from the source to the destination through reconfigurable devices called ROADMs placed at each node in the network. They are basically multiplexers that can select a certain wavelength and, depending on how they are programmed, let it pass through or redirect it. However, these devices, based on wavelength selective switches (WSS), act as cascading filters on the signal that is crossing the network, and the penalty caused by them in real systems cannot be neglected. This thesis

aims to examine and compare different techniques based on multi-subcarrier (MSC) to mitigate the impact of filters on the transmitted signal. The following chapters will study the impact of WSS filtering on single-carrier and MSC systems based on Uniform QAM Constellation and on PCS. In case of MSC, further optimization strategies are investigated to further improve system performance. The presented scenario is characterized by the parameters below:

- a fixed signal Symbol Rate,  $R_s = 128$  GBaud,
- 2 signal polarizations,
- 2 fixed bit rate values to choose from,  $R_b = 800-1200$  Gbit/s,
- a number of subcarriers  $n_{SC} \in [8, 16, 32, 64]$ .

However, before we get into the simulations and the comments on the results there will be a theoretical parenthesis in which the basic concepts the thesis is based on will be explained. Chapter 2 will therefore be devoted to an overview of the two families of the techniques used for simulations outlined in Chapter 3.

## Chapter 2

# Impact of WSS filtering: a theoretical analysis

### 2.1 Current Scenario

As mentioned Chapter 1, in order to perform wavelength routing dynamically along an optical network, ROADM devices are used. A physical model of them has been proposed in [4], and can be simulated and studied through the following transfer function

$$S(f) = \left[ \frac{\sigma\sqrt{2\pi}}{2} \left[ \operatorname{erf} \left( \frac{B/2 - f}{\sqrt{2}\sigma} \right) - \operatorname{erf} \left( \frac{-B/2 - f}{\sqrt{2}\sigma} \right) \right] \right]^{N_{WSS}} \quad (2.1)$$

The variables playing a role in equation 2.1 are: the bandwidth  $B$  of the rectangular aperture in frequency, the number of WSS  $N_{WSS}$  present in the cascade along the line, and the standard deviation  $\sigma = BW_{OTF}/(2\sqrt{2\log 2})$ . The standard deviation depends on  $BW_{OTF}$ , the -3dB bandwidth of the Gaussian-shaped optical transfer function (OTF) of the device. In this thesis, we consider  $B = 134.375$  GHz, a large value, since the considered symbol rate is 128 GBaud and  $BW_{OTF} = 10.4$  GHz according to today's available technology. The number of inserted cascaded filters, instead, will be chosen in  $N_{WSS} \in \{0, \dots, 10\}$  that corresponds to a cascade up to 5 ROADMs since usually one ROADM requires 2 WSS filters, one at the input, to select the incoming lightpath, and one at the output, to choose the output lightpath. Fig. 2.1 shows the transfer functions up to 10 cascaded WSS, where it can be observed that as the number of cascaded WSS increases, the transfer function becomes narrower and narrower, penalizing frequencies at the edges symmetrically.

As previously mentioned, the first differentiation of channel modulation can be made between single carrier modulation and multi-subcarrier modulation. In the simulation analysis that will be presented in the following chapter, we compare SC

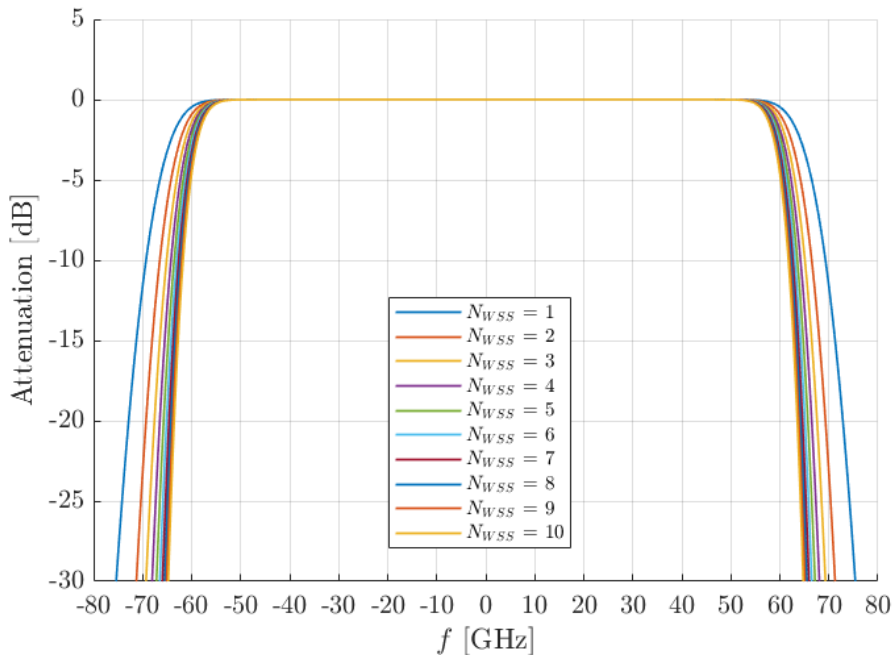


Figure 2.1. Transfer functions of cascaded WSS for  $N_{WSS} \in \{0, \dots, 10\}$  units given by expression 2.1, where  $B = 134.375$  GHz and  $BW_{OTF} = 10.4$  GHz.

and MSC approaches, trying to see if MSC can outperform SC. Deployed optical communication systems operate in single carrier transmitting  $2^M$ -QAM constellations with increasing order  $M$  to obtain higher capacity. In Fig. 2.2 an example of filtering effects on a 128 GBaud single-carrier signal induced by 10 cascaded WSSs is depicted. From there we can see that, although only the edge frequencies are more impacted, an overall decrease of signal quality will be experienced at the receiver. However, in recent years, data traffic has become more heterogeneous, and modulations must be increasingly flexible and able to adapt the data-rate with finer granularity. For this purpose, multi-subcarrier modulation has been considered. In this case, the signal spectrum is sliced into  $N_{SC}$  subcarriers, each working at  $1/N_{SC}$  of the total symbol rate. The filtering effects, in this case, will be symmetrically stronger for the outer subcarriers and almost null for the innermost ones, as can be seen from Fig. 2.3.

Thus, once the number of cascaded filters  $n_{WSS}$  is fixed, it is possible to calculate for each SC its incurred attenuation. By subtracting these attenuation values (a vector of size  $1 \times n_{SC}$ ) from the channel SNR, a vector of SNR per SC is obtained. This vector is used by Uniform QAM Constellation and PCS techniques in their optimization algorithms.

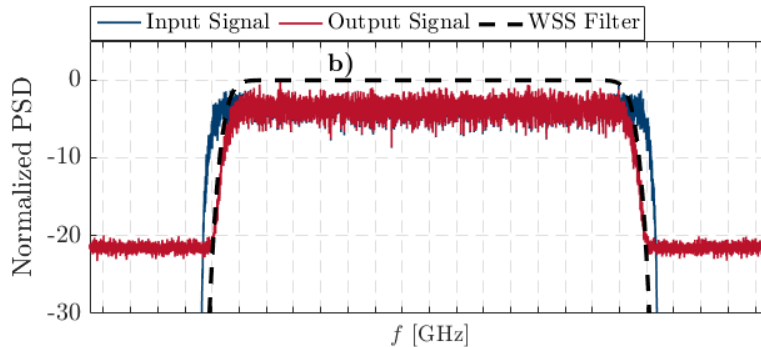


Figure 2.2. Example of filtering effects on a 128 GBaud single-carrier signal due to 10 cascaded WSSs

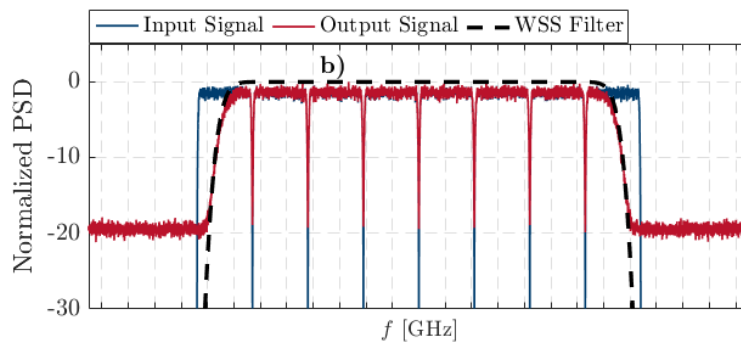


Figure 2.3. Example of filtering effects on a 128 GBaud multi-subcarrier signal due to 10 cascaded WSSs

## 2.2 Uniform QAM Constellation

The subcarrier approach can be exploited through different techniques, in general it is possible to assign different modulation formats or different power levels between the central subcarriers, untouched by the filter, and the outer subcarriers, whose signal will surely be degraded by filtering [5].

Let's start by mentioning a few useful definitions about subcarriers and strategies for determining the necessary modulation format:

- *SNR*, Signal to Noise Ratio, a metric of quality of the transmitted signal, which is defined as the ratio between its power and the power of the noise floor.

$$SNR = \frac{P_{SIGNAL}}{P_{NOISE}} \quad (2.2)$$

it is usually considered in decibels and the formula changes into

$$SNR_{dB} = P_{SIGNAL_{dBm}} - P_{NOISE_{dBm}}, \quad (2.3)$$

- *PR*, Power Ratio, is the ratio between the power of the  $k$ -th subcarrier and the average power of the overall FDHMF signal

$$PR_k = \frac{P_{SC,k}}{P}, \quad (2.4)$$

- *SNR per subcarrier*, can be obtained by

$$SNR_k = PR_k SNR, \quad (2.5)$$

- *BER*, Bit Error Rate, is a key parameter to take into account for Uniform QAM Constellation strategies and it is defined as the ratio between wrongly received bits and transmitted bits Moreover, it can be defined for each sub-carrier and fo the  $k$ -th subcarrier, it is given as:

$$BER_{SC,k} = \Psi(SNR_{SC,k}, M_k), \quad (2.6)$$

where  $\Psi$  is a non-linear function depending on the geometry of the constellation  $M_k$ . For square and cross QAM formats can be approximated using the  $\text{erfc}(\cdot)$  complementary function.

Uniform QAM Constellation’s strategies to mitigate the effect of filters on the signal are mainly based on adjusting the power ratio or modulation format for SC and can be divided into:

- *Same Power*: there is no power difference between the subcarriers, so  $PR_k = 0$  dB for all the  $N_{SC}$ . Therefore, all subcarriers have same power and same modulation format.
- *Power Loading (PL)*: at first, the  $SNR_k$  vector is computed considering the general SNR and the filter attenuation in each subcarrier. Then, the vector of  $PR_k$  defined over the subcarriers is iteratively optimized in order to minimize the BER exploiting the `fminsearch` Matlab function. As a result, a lower PR will be obtained in the central SCs and a higher PR in the outer SCs, which have to compensate for a stronger filtering effect.
- *Bit Loading (BL)*: after computing the  $SNR_k$  vector as before, the algorithm generates, choosing from an initial set of constellation cardinality  $M$ , all possible hybrid combinations which maintain an imposed average number of bits per symbol. Then, for each of them, the total BER is computed from theory. Finally, the decision is made choosing the configuration associated to the minimum BER. For example using 8 subcarriers, given [4 8 16 32 64 128] as initial set and  $R_s = 1.2T$  as the symbol rate to meet and the constraint of symmetry, the possible combinations are reported in table 2.1.

- *Bit & Power Loading (BPL)*: Both the above strategies are applied. Specifically, at first, the optimal  $PR_k$  are found then, all hybrid combinations are generated and the best one is chosen, both decisions are based on the minimum BER criterion as before.

SC 1	SC 2	SC 3	SC 4	SC 5	SC 6	SC 7	SC 8
8	128	128	128	128	128	128	8
16	64	128	128	128	128	64	16
32	32	128	128	128	128	32	32
32	64	64	128	128	64	64	32
64	64	64	64	64	64	64	64

Table 2.1. Hybrid Bit Loading combinations.

The last two strategies are characterized by assigning different modulation formats to each SC, this technique is called Frequency-Domain Hybrid Modulation Formats (FDHMF) and makes it possible to adjust spectral efficiency with fractional granularity and to enhance the tolerance towards filtering caused by ROADMs.

## 2.3 Probabilistic Constellation Shaping

Another type of modulation approach for subcarriers is the one that exploits the Probabilistic Constellation Shaping (PCS) technique, which has the great advantage of being able to provide an arbitrary granularity of the Bit Rate.

When considering the PCS, we need to provide the reader some useful definition from Information Theory that will come into play in the discussion of the analyzed optimization strategies.

- *Entropy*, usually identified with the letter  $H$ , tells how much information rate can be sent along the channel, for Uniform QAM Constellation the entropy is fixed to the constellation order chosen and is equal to the number of bits per symbol:

$$H = \log_2 M \tag{2.7}$$

For PCS instead, as it will be further explained later, it is only determined by the probability distribution of the source modulator, meaning that a set of input bits are modulated onto the QAM alphabet according to a probability function  $P(X)$ . In this case the entropy is defined as:

$$H(x) = \sum_{i=1}^M P(x_i) \log_2 P(x_i) \tag{2.8}$$

- *Capacity*,  $C$ , is the maximum information rate the channel can transport and is independent of the type of modulation:

$$C = \log_2(1 + SNR) \quad (2.9)$$

- *Mutual Information*,  $MI$ , namely  $I(X; Y)$ , is a quantity measuring the relationship between two random variables  $X$  and  $Y$ , in other words, tells how much information is communicated in one random variable about the other. Its formula for discrete variables with joint probability  $P_{XY}(x, y)$  is:

$$I(X; Y) = \sum_{x,y} P_{XY}(x, y) \log \frac{P_{XY}(x, y)}{P_X(x)P_Y(y)} \quad (2.10)$$

MI has also another intuitive interpretation as the useful size of a message and is counted in units of bits. In fact, if the entropy is a measure of the uncertainty of a variable  $X$ , MI tells instead the reduction in uncertainty:

$$MI = MI(X, Y) = H(X) + H(Y) - H(X, Y) \quad (2.11)$$

where  $H(X)$ ,  $H(Y)$  and  $H(X, Y)$  are entropies respectively defined with the distributions  $P_X$ ,  $P_Y$  and  $P_{X,Y}$ .

- *Normalized Generalized MI (NGMI)*, is the metric commonly utilized to provide a universal assessment of achievable information rate for any modulation format, is defined as [6]

$$NGMI = 1 - \frac{G(M_{PCS}, P_x, \sigma^2)}{\log_2(M_{PCS})}, \quad (2.12)$$

where  $G(\cdot)$  represents the information loss due to propagation over the AWGN channel, defined as:

$$G(M_{PCS}, P_x, \sigma^2) = \frac{1}{N} \sum_{n=1}^N \sum_{k=1}^{\log_2(M_{PCS})} \log_2 \frac{\sum_{x_m \in \chi} \exp(-\frac{|y_n - x_m|^2}{\sigma^2}) P_{x_m}}{\sum_{x_m \in \chi(k, b_n, k)} \exp(-\frac{|y_n - x_m|^2}{\sigma^2}) P_{x_m}} \quad (2.13)$$

- $OH$ , is the FEC overhead, it measures the number of redundant information that allows the receiver to detect and correct the received message.
- $R_b$ , is the net target Bit Rate of the transmitted signal, and is a function of

$$R_b = f(M, OH, R_s, \lambda), \quad (2.14)$$

where  $R_s$ , the symbol rate, and  $M$  are set, while the  $OH$  and  $\lambda$  are not fixed. A more detailed definition has been presented in [6]:

$$R_b = 2R_s[2 - (1 - R_{FEC}) \log_2 M + R_{DM}(\log_2 M - 2)], \quad (2.15)$$

where  $R_{FEC}$ , the FEC rate, and  $R_{DM}$ , the rate of the Distribution Matcher [6], are given by:

$$R_{FEC} = \frac{1}{1 + OH}, \quad R_{DM} = \frac{H_{PCS} - 2}{\log_2 M - 2}, \quad (2.16)$$

the only parameter left,  $\lambda$ , is included in the definition of  $H_{PCS}$ , calculated as illustrated in 2.8 with a probability distribution function  $P(x)$  that will be introduced in a little while (Eq. 2.17) and that depends on  $\lambda$ .

Graphically representing the above formula, where the fixed parameters  $R_s$  and  $M$  are set respectively to 128 GBaud and 64, it is possible to visualize the different achievable bit rate values, represented in different curves in 2.4. However, in the following of this thesis also the OH parameter is fixed at the

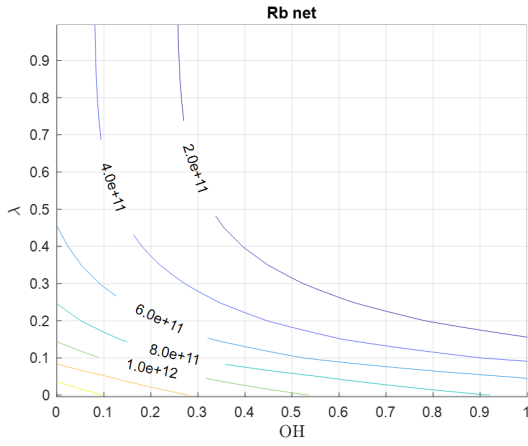


Figure 2.4. Bit Rate curves.

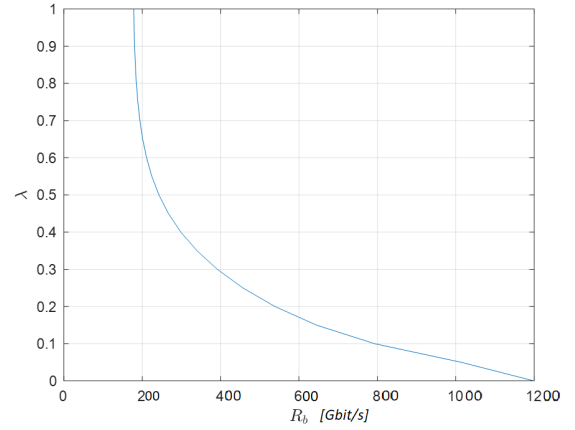


Figure 2.5.  $\lambda$  vs  $R_b$ .

value of  $OH = 0.28$ , this is equivalent to drawing a vertical line in the figure 2.4 allowing lambda to be expressed as a function of  $R_b$ , as can be observed in 2.5.

The concept of PCS lies in assigning a probability distribution to the symbols of a starting constellation in order to adjust entropy and bit rate. Therefore, instead of a uniform distribution among the constellation points, PCS usually assigns the Maxwell-Boltzmann distribution, whose expression is reported in Eq. 2.17 to form a Gaussian-like constellation:

$$P_{x_n} = \frac{\exp(-\lambda|x_n|^2)}{\sum_{n=1}^{M_{PCS}} \exp(-\lambda|x_n|^2)}, \quad (2.17)$$

where  $\lambda \geq 0$  is called the shaping parameter and tells how much the PCS constellation is shaped with respect to the original square  $M_{PCS}$  one. When is set to 0 the

Maxwell-Boltzmann converges to a uniform distribution.

An example is provided in Fig. 2.6, where are shown different levels of shaping corresponding to a range of bit rates from 600G to 1200G achievable from the same starting modulation format  $M_{PCS} = 64$ . It is noticeable that 1200G is the maximum obtainable bit rate since the 64-QAM constellation is not shaped at all (this corresponds to a  $\lambda = 0$ ), whereas the more shaped is the constellation, the higher the value of lambda. The constellation points with higher probability can also be seen in the figure 2.7 where the decoded points at the receiver are shown in a scatter plot in the I-Q plane.

PCS also allows for minimization of the average signal energy increasing the shaping gain  $G_{PCS}$ , defined as the ratio between the energies of the symbol from the shaped constellation and the respective uniform QAM one:

$$G_{PCS} = 10 \log_{10} \left( \frac{\sum_n^{M_{QAM}} |u_n|^2}{\sum_k^{M_{PCS}} |s_k|^2 P_{sk}} \right) \quad (2.18)$$

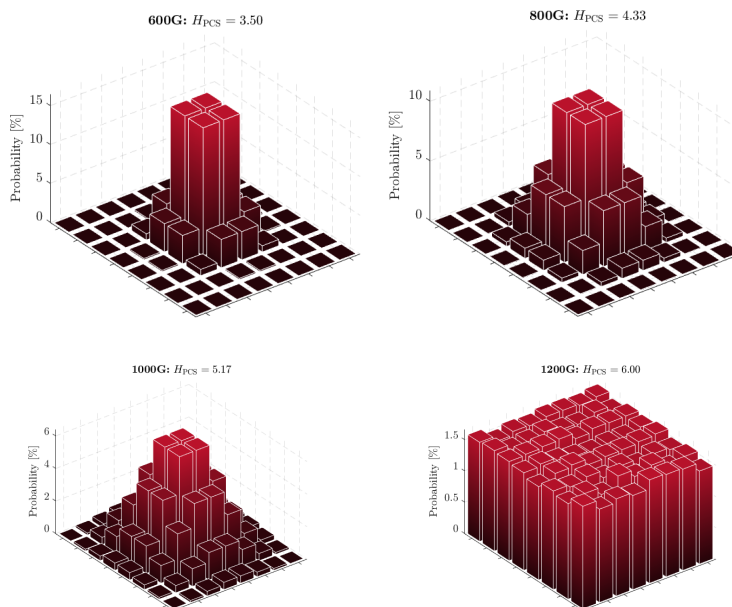


Figure 2.6. Probability density functions of PCS constellations for different shaping levels.

As done for the Uniform QAM Constellation case, the optimization strategies considered for PCS are below listed and explained:

- *Same Power*, the simplest and most basic one, as before, all SCs are assigned with the same power, so  $PR_k = 0$  dB. The shaping level, thus the  $\lambda$  value, is

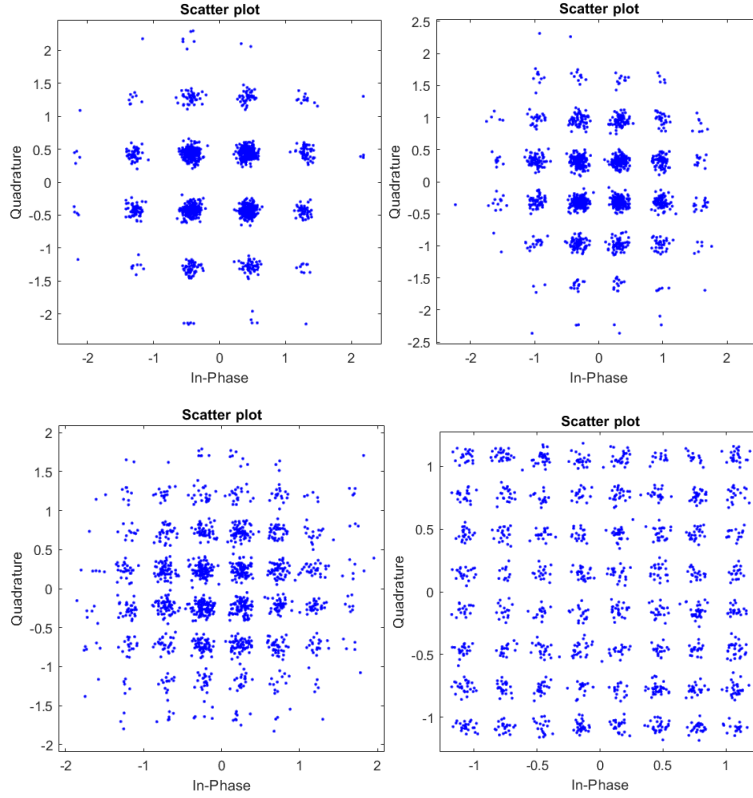


Figure 2.7. Scatter plot of the constellation point at the Rx.

decided purely on the basis of the imposed bit rate since, as it's possible to read in [6], the entropy required by the PCS to reach a certain bit rate is:

$$H_{PCS} = \frac{R_b}{2R_s + H_{FEC}}, \quad (2.19)$$

where the other parameters are the symbol rate  $R_s$  and the entropy that must be allocated for the FEC parity bits  $H_{FEC}$ . The following step after finding the value of entropy is to calculate the respective value of  $\lambda$ , this is done through a fitting function of the Maxwell-Boltzmann probability distribution. The same  $\lambda$  value is then assigned to all the SCs.

- *Entropy Loading*, the aim is to assign the optimum  $\lambda$  value to each subcarrier. This is done to make the transmission more efficient since each subcarrier is differently impaired by the WSS filtering, thus each of them has a different  $SNR_k$ . The steps of the algorithm are further explained below.
- *Water Filling*, an optional feature, in our case used together with EL, to optimize power allocation in a transmission channel. This technique, which

is a fundamental achievement in information theory, was originally derived by Shannon in 1949 [8]. The basic idea, as illustrated in fig 2.8 is to allocate more power to the frequencies with less noise and reduce it to the more penalized ones. With WSS this translates into redistributing the SNR by reducing it in the outer SCs, those most filtered, and increasing it in the inner SCs, which are less damaged by the filter.

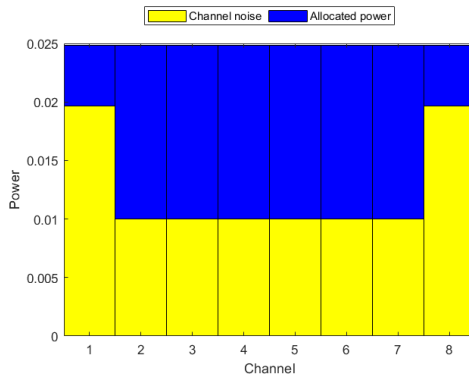


Figure 2.8. Power redistribution according to the Water Filling technique

### 2.3.1 Entropy Loading algorithm

The EL algorithm is repeated for each considered number of cascaded WSS and for every SNR value inserted. It is executed ahead of the time-domain simulation because the idea is to find the optimum  $\lambda$  vector and then pass it to the transmitter. The steps of the developed EL algorithm are the following:

1. First of all, the algorithm computes the impact of WSS filtering on the subcarriers in terms of SNR level. So, given an initial SNR value for the channel, a vector of SNR per subcarrier,  $SNR_{SC}$  is computed.
2. Then the Waterfilling optimization is applied to the SNR vector retrieving a new vector,  $SNR_{SC_{WF}}$ , with optimized SNR values.
3. This step retrieves an entropy value for each SNR in the  $SNR_{SC_{WF}}$  vector. The passage is done through a Look Up Table (LUT), acquired by Monte-Carlo simulations, storing the relations between NGMI, SNR and entropy, illustrated in figure 2.9. The NGMI value, according to the study presented in [9], is set to 0.9. The entropy value is then found through an iterative search that aims to find the value of entropy that is the closest to the inserted SNR. This search is done for all the subcarriers, so the output of this function is an entropy vector,  $H_{SC}$ .

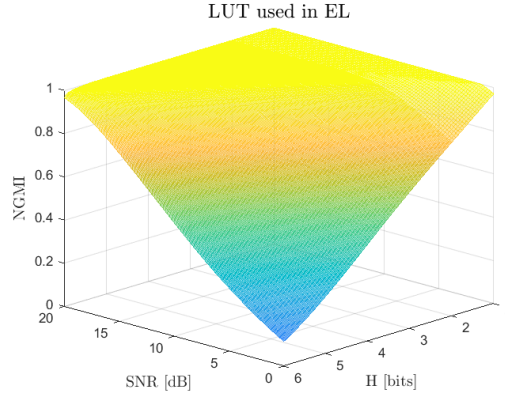


Figure 2.9. Look Up Table storing the relations between NGMI, SNR and H.

4. As last step, using a fitting algorithm on the Maxwell-Boltzmann probability distribution, a  $\lambda$  value is retrieved from each entropy. The final  $\lambda_{SC}$  vector, optimal for the initial considered SNR, is found.

The same steps are reported through the following example. Considering a system with these characteristics:

$$\begin{aligned} M_{PCS} &= 64, \\ n_{SC} &= 8, \\ SNR_{dB} &= 13, \\ n_{WSS} &= 10. \end{aligned}$$

1. The impact of WSS filtering on subcarriers in terms of SNR level is:

$$SNR_{SC_{dB}} = [10.066 \quad 12.999 \quad 13.000 \quad 13.000 \quad 13.000 \quad 13.000 \quad 12.999 \quad 10.066], \quad (2.20)$$

as was stated in the previous chapter, the effect of the filter is symmetrical with respect to the 8 subcarriers.

2. The vector is optimized through the water filling technique:

$$SNR_{SC_{WF}} = [9.905 \quad 13.051 \quad 13.052 \quad 13.052 \quad 13.052 \quad 13.052 \quad 13.051 \quad 9.905] \quad (2.21)$$

It is noticeable that there is a slight increase in the central SNRs and likewise a modest decrease in the outer ones.

3. The entropy per subcarrier is searched through the LUT:

$$H_{SC} = [3.9103 \quad 4.8838 \quad 4.8839 \quad 4.8839 \quad 4.8839 \quad 4.8839 \quad 4.8838 \quad 3.9103], \quad (2.22)$$

4. The  $\lambda$  values are derived from the entropies:

$$\lambda_{SC} = [0.1420 \quad 0.0704 \quad 0.0704 \quad 0.0704 \quad 0.0704 \quad 0.0704 \quad 0.0704 \quad 0.1420], \quad (2.23)$$

Consistently with what was stated above, the external constellations will be more shaped, as the corresponding subcarriers will carry less information.

In this way the  $\lambda_{SC}$  vector, considered the optimum for the  $SNR_{dB} = 13$  and  $nWSS = 10$  case, has been computed. The same process is done for all the other SNR values. Then, in the time-domain simulation, for every tested SNR, the corresponding  $\lambda$  vector is used in the transmitter to optimize the constellation shaping.

## Chapter 3

# Simulation Results

The system analyzed in this thesis considers zero optical fiber length to connect the transmitter and receiver. This type of configuration is usually used in simulations and tests since it eliminates the effects of the transmission medium, to study the impairments brought by a particular source, in our case the cascade of WSS. This means that the impacts of attenuation and dispersion, briefly introduced in Chapter 1, were not taken into consideration. The implemented system is characterized by high values of both symbol rate,  $R_s = 128$  GBaud, and bit rates,  $R_b = 800$ -1200 Gbit/s, so the bandwidth of the signal is larger. This results in choosing WSS filters with a larger 3dB bandwidth, in fact  $B = 134.375$  GHz. Increasing the bit and symbol rates also gives the possibility of using a rather large number of SCs, in fact, the simulations performed consider a number of SC ranging from 1, thus the single carrier case, up to a maximum of 64. The choice of such a high number of SCs is due to the fact that, as it has been demonstrated in several works, [10] and [11], to reduce the impact of nonlinearities the optimum symbol rate per SC has to be found in the of 2-4 GBaud range, which corresponds to having 64 and 32 subcarriers, respectively. The results presented below are obtained either from theoretical calculations or from a time-domain simulation. The theoretical analysis is a sort of "spectral-domain" simulation, since, given the signal spectrum and the WSS attenuation, it derives SNR from which one can calculate the BER analytically. While in the time-domain simulation a number of symbols are created and transmitted following the steps explained in the DSP description in Chapter 1. BER in this latter case is actually calculated by comparing received bits with transmitted bits. The theoretical analysis is necessary to understand whether it can be used in the design/optimization of the modulation strategies presented.

### 3.1 BER and MI

At the end of each time-domain simulation, transmission performance is measured by computing the *BER* and the *MI*, as anticipated. These are two different approaches that allow setting thresholds below which the transmission cannot be considered acceptable, so both methods provide a way to derive the minimum SNR needed to meet the threshold. The BER calculation is done at the bit level since you have to count the wrong received bits and relate them to the total received bits, so it can only be applied to the Uniform QAM Constellation. In case of PCS, on the other hand, where points in the constellation have different probabilities of occurrence, BER loses its meaning and the only metric to be exploited is MI, which indicates the amount of information carried and is calculated from the symbols. The steps in both cases are the same: after fixing the number of cascaded WSS, the BER or MI is calculated for each SNR value set at the input, and the resulting curve will then be cut at the set threshold, thus deriving the corresponding required SNR.

Figures 3.1 and 3.2 show the BER and the MI, respectively, with respect to SNR

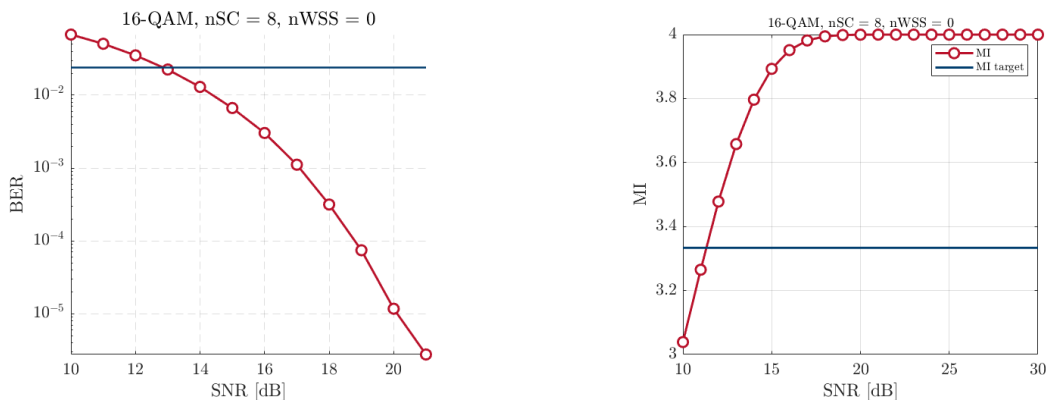


Figure 3.1. BER values for a transmission with 8 subcarriers and without filters Figure 3.2. MI values for a transmission with 8 subcarriers and without filters

levels in case of zero WSS and 8 subcarriers assuming 16QAM modulation format for all subcarriers. Also their corresponding BER and MI target are reported. For this thesis the BER target is set to 0.024, while the MI target is 3.33 in the 800G configuration and 5 for the 1.2T system. The first thing that can be noticed by looking at the two curves is that, as the SNR increases, the BER curve decreases while the MI one increases. That happens because, giving more power to the input signal, the transmission will be more reliable and with fewer erroneous bits. The MI curve, on the contrary, increases with the SNR until it saturates at the maximum entropy value reachable by the considered constellation, in this case 16-QAM, thus  $\log_2(16) = 4$ .

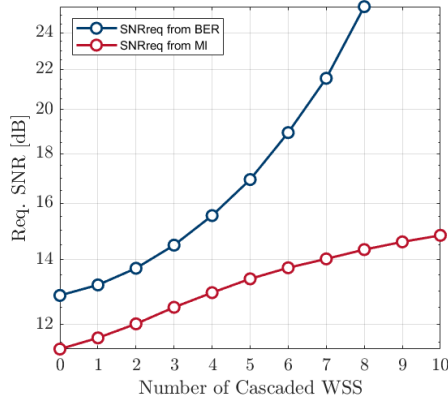


Figure 3.3. Required SNR obtained from both BER and MI.

Another observation that can be noted from figures 3.1 and 3.2 is that the respective required SNRs have different values:  $SNRreq_{BER} \simeq 12.86$  and  $SNRreq_{MI} \simeq 11.32$ . This difference is more observable in fig. 3.3 in which the obtained required SNR curves are compared for all values of nWSS from 0 to 10. Therefore, it can be concluded that these two metrics are equivalent but not comparable. In fact, throughout the thesis, graphs comparing Uniform QAM Constellation and PCS will both be derived using MI.

Figures 3.4, 3.5 and 3.6 compare instead the BER obtained theoretically by subtracting the effect of filter attenuation from the imposed SNR and the BER computed from the time-domain simulation; as expected, for all the three graphs, the theory performs better than the actual simulation since the blue curve always remains below the red one. However, it is evident that as the number of WSS increases, the two curves diverge more and more from each other. In the case without filters (fig. 3.4) the theoretical and the simulation curves almost overlap, making the theory an accurate prediction of the time-domain simulation. This behaviour is not followed at all by the curves in figures 3.5 3.6 in which it is evident that the theoretical BER cannot be considered a prediction of that obtained by simulation. This strong difference between the two curves also leads to prediction error in SNR-req, as visible in Figure 3.7, where theory and simulation start with less than 1 dB gap and then diverge widely as WSS increases. This trend is coherent with what explained in [5], namely that in order to simplify the theoretical calculation of BER, or MI, the WSS filter transfer function is approximated by a polynomial of degree 0, meaning that within each subcarrier the transfer function is flat while there is a step variation between different subcarriers. This simplification is the reason why theory appears to perform better than simulation: in each subcarrier the attenuation level is set according to the average power loss; later it will be shown also that, as a consequence, increasing the number of subcarriers, the approximation will be

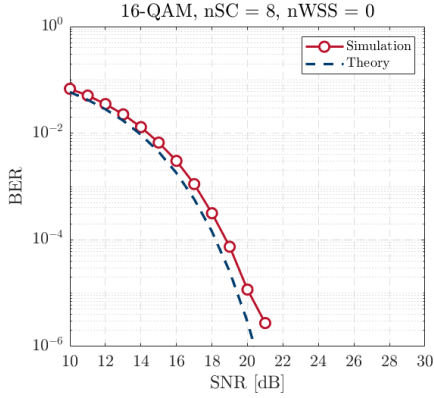


Figure 3.4. Comparison of BER theory and BER simulated, without filters.

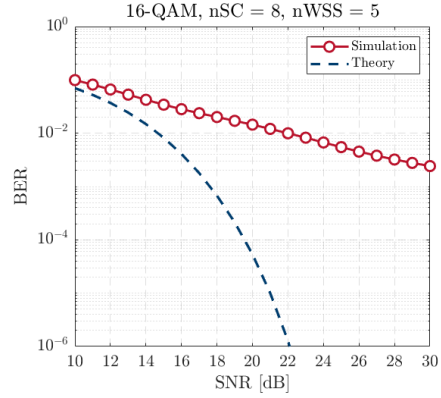


Figure 3.5. Comparison of BER theory and BER simulated, with 5 filters.

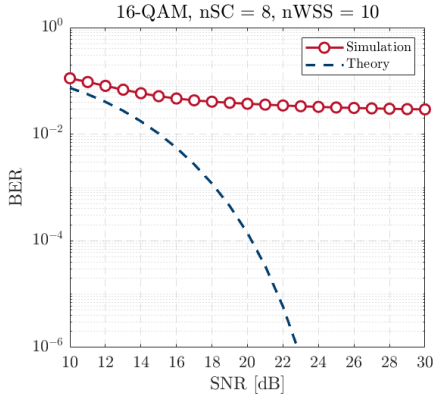


Figure 3.6. Comparison of BER theory and BER simulated, with 10 filters.

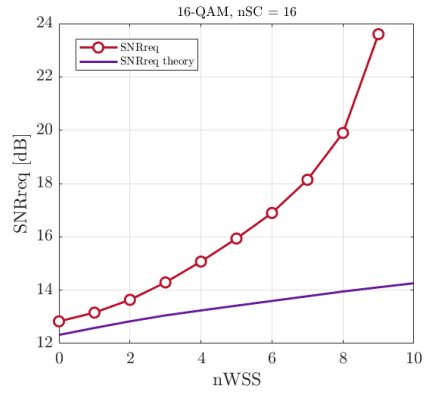


Figure 3.7. Comparison between theoretical and simulated required SNR.

closer to the real WSS transfer function 2.1, leading to a better approximation. Developing Figures 3.1 and 3.2 by simultaneously plotting all the curves obtained with a number of WSS from 0 to 10, we obtain Figures 3.8 and 3.9, which show how a stronger filtering affects BER and MI. Again, if BER curves rise as nWSS increases, MI curves fall (purple curve in both cases); this behavior is predictable and consistent with what was said earlier: adding impairments to the signal implies a bit's error increase and a carried signal's information decrease.

A further consideration to be made is based on how, in both cases, the curves are cut by the targets, as this leads to different behaviors. The MI target (fig. 3.9) is able to cut all the MI curves at low SNR values, below SNR = 15 dB; it follows that the required SNR values will be found for all the 11 selected nWSS values (from 0 to 10) and that the range of SNRs to be tested can be shortened allowing faster simulations. On the contrary, this is untrue for the BER since not all the curves intersect with the target BER line given that they tend to floor as the SNR

increases (fig. 3.8). In order to be able to achieve the required SNR for curves with 9 and 10 WSS, the imposed range of SNRs must be extended without knowing the sufficient upper bound, thus leading to much longer simulations.

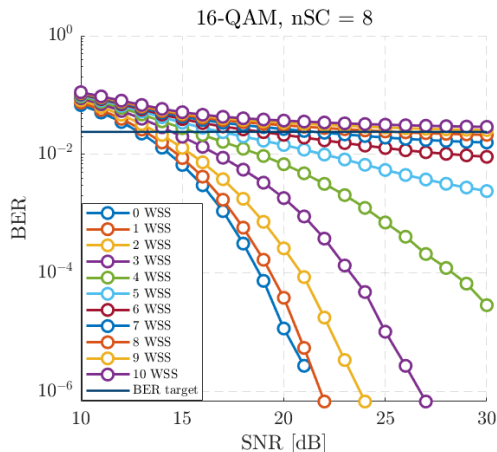


Figure 3.8. BER values for a transmission with 8 subcarriers and filters  $nWSS \in \{0, \dots, 10\}$

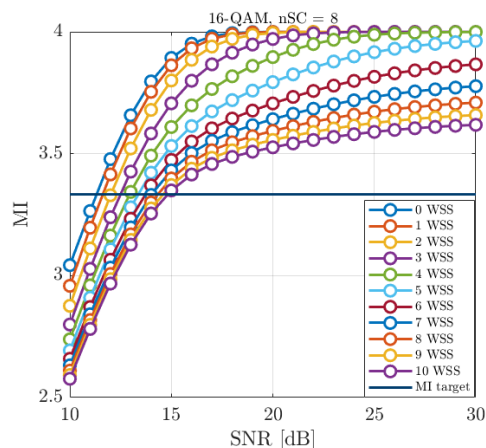


Figure 3.9. MI values for a transmission with 8 subcarriers and filters  $nWSS \in \{0, \dots, 10\}$

## 3.2 Uniform QAM Constellation Comparison

Let the analysis of simulations results begin by focusing only on Uniform QAM Constellation highlighting the advantages and disadvantages of utilizing multi-subcarriers with the related techniques already presented and explained in Chapter 2. The following results have been obtained considering the BER as performance metric. Figure 3.10 provides an overview of modulation techniques for Uniform 16-QAM constellation with 800G total bit rate applied in four different systems that have, in order, 8, 16, 32 and 64 subcarriers. It is important to underline that the four techniques presented in Chapter 2, Same Power, Power Loading, Bit Loading and Bit & Power Loading, are always compared with the single carrier case, as the purpose is to see under which conditions the multi-subcarrier approach is able to provide an advantage over the "traditional" case. The first thing that can be noticed is that, as it ought to be, in the unfiltered condition all cases get the same required SNR, in other words all curves start from the same point regardless of the number of subcarriers or the considered technique. From the graphs, the single carrier turns out to be, for the majority of cases, better than considering MSC jointly with other optimization techniques. The black curve, in fact, generally lies below the others since it benefits from lower SNRreqs for the same number of cascaded

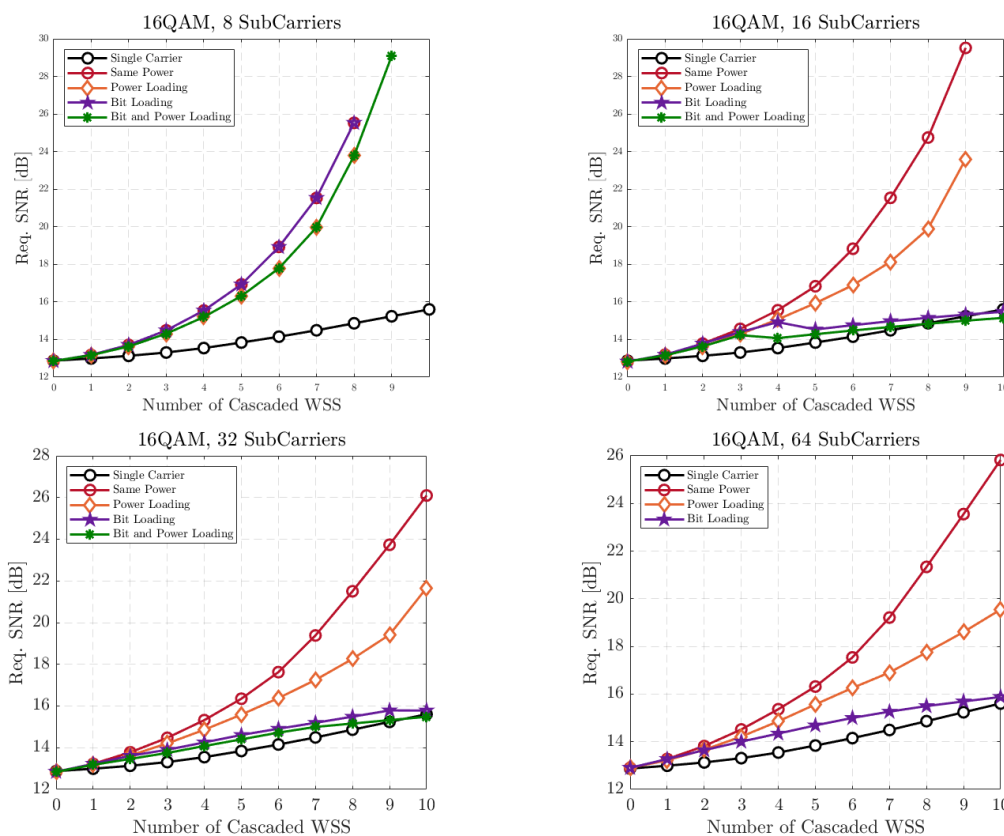


Figure 3.10. Comparison of techniques using 16-QAM with  $n_{SC} = 8, 16, 32, 64$ .

filters. Observing the top-left plot and comparing it with the others, it can be clearly concluded that it is the worst case performance of multi subcarriers with respect to the 16-QAM single carrier version. Better performances are obtained as the number of subcarriers increases. A closer look at the curves shows that in the first graph the technique optimizing the power per subcarrier, i.e. power loading (PL), is able to achieve slightly better results than the others, but from 16 subcarriers and more, it is clearly outperformed by Bit Loading. Instead, the technique that performs both Bit & Power Loading, in each case turns out to be the best. However, its computational cost and time required for the optimization exceed those of the others consistently, especially with a large number of subcarriers.

Now the same set of graphs made with a higher order modulation 64-QAM and 1.2 T of overall bit rate, will be analyzed. Figure 3.11 shows, as expected, generally higher required SNR values compared to the values obtained in case of 800G transmission. Indeed, the larger the cardinality of a modulation, the higher the required signal-to-noise ratio, which is why, in cases of poor transmission quality, we return

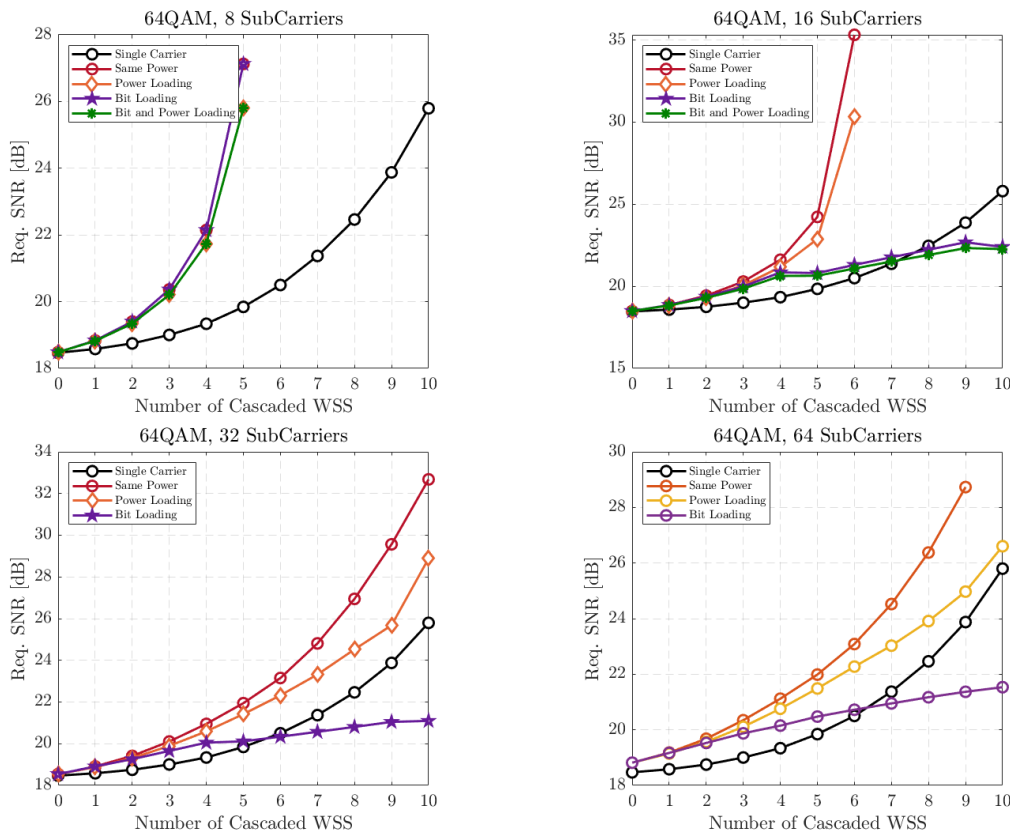


Figure 3.11. Comparison of techniques using 64-QAM with  $n_{SC} = 8, 16, 32, 64$ .

to the use of more simple and robust modulations such as 4-QAM. It is evident from the first plot that even with 64-QAM the 8 subcarriers configuration is not suitable since none of the techniques approaches the single-carrier reference curve. However, the other graphs configurations prove to be more advantageous than the respective ones in figure 3.10, in fact with 32 subcarriers the Bit Loading technique already crosses the black single-carrier curve for a number of WSS equal to 6. Additionally, in the last two plots the Bit & Power Loading curves are missing, this is a consequence of the aforementioned issue, i.e., the excessive computational cost of this technique which is definitely a major drawback compared to the minimal advantage it brings over Bit Loading.

To further investigate the comparison between the MSC and single carrier cases, those techniques that from the previous graphs were found to be advantageous were collected in the graph in figure 3.12, which considers a wider range of  $n_{WSS}$  from 0 to 16; the uppermost bundle of curves is related to 64-QAM, while the bottom one to 16-QAM. In this graph we clearly see the intersections between the MSC and single carrier curves, verifying that the trend of those lines crossing the reference

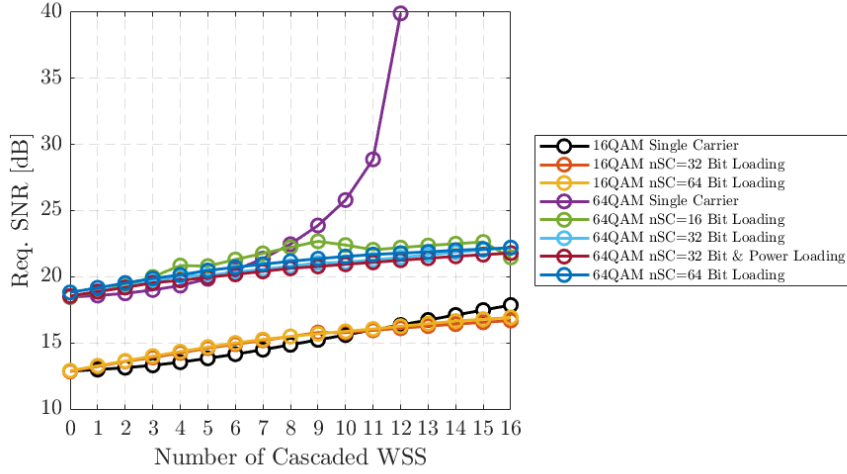


Figure 3.12. Bit Loading and Bit and Power Loading applied up to 16 WSSs for different nSC and M-QAM.

one does not change but remains smooth. Therefore, if a technique turns out to be better than single carrier for a certain number of cascaded filters, then it will be better than it for any higher number. From this perspective, the advantage brought by MSC when used with 64-QAM modulation is even more evident, in fact it turns out to be of several dBs, in contrast to that of 16-QAM modulation which achieves maximum 1 or 2 dB of advantage only with 16 cascaded WSS.

From the previous graphs it was possible to learn how, for the same number of subcarriers, the modulation technique affects the minimum SNR value necessary to guarantee a BER threshold. It is clear that 8 subcarriers are not sufficient neither in the 16-QAM configuration nor, especially, with 64-QAM. In fact, by doing the maths, the symbol rate per subcarrier  $R_{sSC}$  in the 8 subcarriers configuration reaches  $(800 * (1 + 0.28)) / (\log_2(16) * 2 * 8) = (1200 * (1 + 0.28)) / (\log_2(64) * 2 * 8) = 16$  GBaud, a value significantly high. In the above formula 0.28 is our system's Overhead and the multiplication by 2 is done since we are considering the two signal's polarization. By analyzing Figures 3.13 - 3.20, where different subcarrier numbers are compared for each modulation technique, the clear inferiority of the 8 SC is evident in all cases. Instead, when the number of subcarriers is 16, the behavior is good with Bit Loading and Bit & Power Loading (fig. 3.15, 3.16, 3.19, 3.20) but continues to be weak for Same Power and Power Loading (fig. 3.13, 3.14, 3.17, 3.18), again, doing the same previous calculations changing the number of SC from 8 to 16, we get 8 GBaud, still out of the optimum range. The only configurations that remain within the range are 32 and 64 subcarriers, in fact in all figures we see how their performance is better than the other curves, especially in the cases of

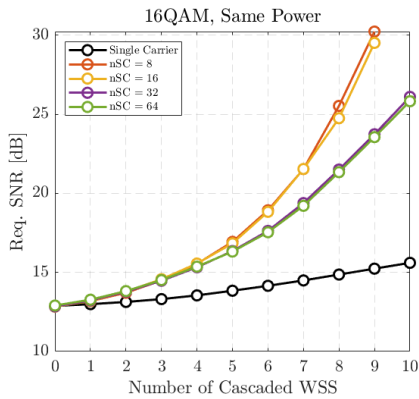


Figure 3.13. Comparison of nSC for 16-QAM applying Same Power.

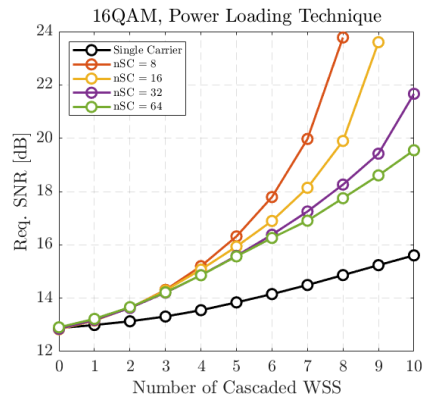


Figure 3.14. Comparison of nSC for 16-QAM applying Power Loading.

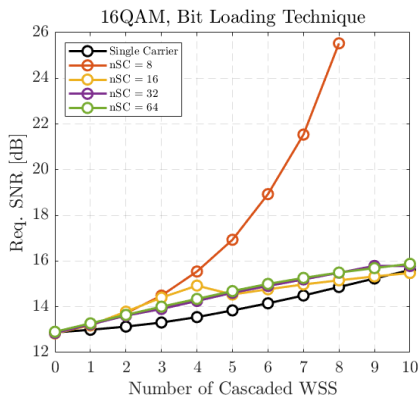


Figure 3.15. Comparison of nSC for 16-QAM applying Bit Loading.

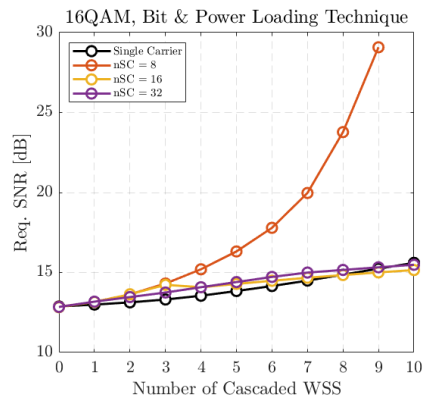


Figure 3.16. Comparison of nSC for 16-QAM applying Bit and Power Loading.

figures 3.19 and 3.20 with 64-QAM. Below, by example, there are tables showing the work of the modulation techniques we have discussed so far. In Table 3.1 it is possible to see how Power Loading acts on the power of each SC by changing its Power Ratio (defined in 2.4); in the upper part the starting SNR of the signal is 20 dB while in the lower part it is 25 dB. Looking at the first row, it can be seen that without filters there is no need to change the power, in fact all PRs are set to 0, however, as the number of cascaded filters increases, the subcarriers on the edges will be increasingly damaged and will need more power to be able to transmit a reliable signal, while the central ones can transmit using less power. The values in the table are in dB; hence, it can be seen that the central subcarriers have negative values, i.e., PR less than 1, while the outer subcarriers have positive values, thus larger than 1.

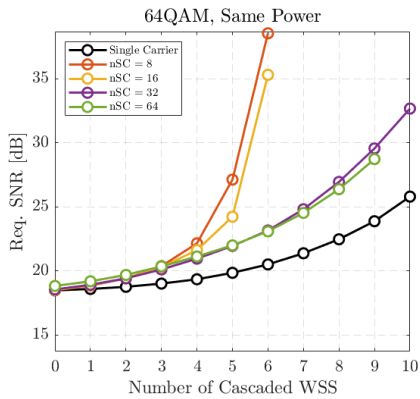


Figure 3.17. Comparison of nSC for 64-QAM applying Same Power.

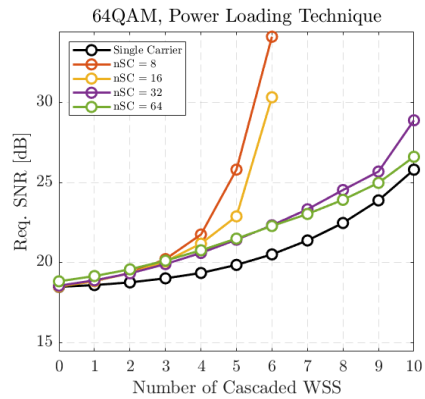


Figure 3.18. Comparison of nSC for 64-QAM applying Power Loading.

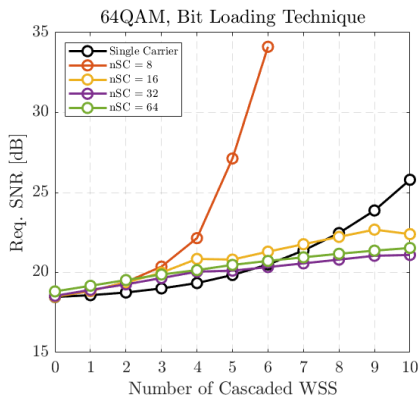


Figure 3.19. Comparison of nSC for 64-QAM applying Bit Loading.

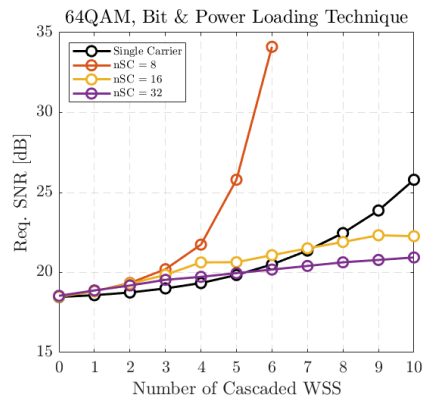


Figure 3.20. Comparison of nSC for 64-QAM applying Bit and Power Loading.

Additionally, the tables 3.2 and 3.2 show the constellations chosen for each subcarrier with the Bit Loading and Bit and Power Loading techniques in the 16-QAM case, as can be seen there are both higher and lower orders of 16, depending on whether the sc is central or external, the important thing being that the overall bit rate is 800G.

Power Ratios per SC								
Power Loading Technique								
SNR = 20 dB								
	SC 1	SC 2	SC 3	SC 4	SC 5	SC 6	SC 7	SC 8
0 WSS	0	0	0	0	0	0	0	0
1 WSS	0.5350	-0.1941	-0.1940	-0.1940	-0.1940	-0.1940	-0.1941	0.5350
2 WSS	0.8703	-0.3337	-0.3338	-0.3336	-0.3336	-0.3338	-0.3337	0.8703
3 WSS	1.0974	-0.4374	-0.4375	-0.4375	-0.4375	-0.4375	-0.4374	1.0974
4 WSS	1.2626	-0.5181	-0.5182	-0.5182	-0.5182	-0.5182	-0.5181	1.2626
5 WSS	1.3911	-0.5842	-0.5841	-0.5841	-0.5841	-0.5841	-0.5842	1.3911
6 WSS	1.4952	-0.6396	-0.6400	-0.6400	-0.6400	-0.6400	-0.6396	1.4952
7 WSS	1.5827	-0.6881	-0.6882	-0.6885	-0.6885	-0.6882	-0.6881	1.5827
8 WSS	1.6580	-0.7310	-0.7312	-0.7313	-0.7313	-0.7312	-0.7310	1.6580
9 WSS	1.7242	-0.7699	-0.7702	-0.7698	-0.7698	-0.7702	-0.7699	1.7242
10 WSS	1.7830	-0.8049	-0.8051	-0.8052	-0.8052	-0.8051	-0.8049	1.7830
Power Loading Technique								
SNR = 25 dB								
	SC 1	SC 2	SC 3	SC 4	SC 5	SC 6	SC 7	SC 8
0 WSS	0	0	0	0	0	0	0	0
1 WSS	0.5742	-0.2095	-0.2096	-0.2098	-0.2098	-0.2096	-0.2095	0.5742
2 WSS	0.9355	-0.3626	-0.3627	-0.3628	-0.3628	-0.3627	-0.3626	0.9355
3 WSS	1.1807	-0.4775	-0.4776	-0.4777	-0.4777	-0.4776	-0.4775	1.1807
4 WSS	1.3600	-0.5678	-0.5680	-0.5679	-0.5679	-0.5680	-0.5678	1.3600
5 WSS	1.4993	-0.6419	-0.6422	-0.6421	-0.6421	-0.6422	-0.6419	1.4993
6 WSS	1.6127	-0.7052	-0.7052	-0.7053	-0.7053	-0.7052	-0.7052	1.6127
7 WSS	1.7078	-0.7601	-0.7605	-0.7603	-0.7603	-0.7605	-0.7601	1.7078
8 WSS	1.7899	-0.8091	-0.8094	-0.8094	-0.8094	-0.8094	-0.8091	1.7899
9 WSS	1.8620	-0.8534	-0.8536	-0.8538	-0.8538	-0.8536	-0.8534	1.8620
10 WSS	1.9264	-0.8941	-0.8943	-0.8943	-0.8943	-0.8943	-0.8941	1.9264

Table 3.1. Power Ratio values applied per subcarriers using the Power Loading Technique, starting from SNR = 20 dB and SNR = 25 dB.

Constellation Formats per SC																
Bit Loading Technique																
	SC 1	SC 2	SC 3	SC 4	SC 5	SC 6	SC 7	SC 8	SC 9	SC 10	SC 11	SC 12	SC 13	SC 14	SC 15	SC 16
0 WSS	16	16	16	16	16	16	16	16	16	16	16	16	16	16	16	16
1 WSS	16	16	16	16	16	16	16	16	16	16	16	16	16	16	16	16
2 WSS	8	16	16	16	16	16	16	32	32	16	16	16	16	16	16	8
3 WSS	8	16	16	16	16	16	16	32	32	16	16	16	16	16	16	8
4 WSS	8	16	16	16	16	16	16	32	32	16	16	16	16	16	16	8
5 WSS	8	16	16	16	16	16	16	32	32	16	16	16	16	16	16	8
6 WSS	4	16	16	16	16	16	32	32	32	32	16	16	16	16	16	4
7 WSS	4	16	16	16	16	16	32	32	32	32	16	16	16	16	16	4
8 WSS	4	16	16	16	16	16	32	32	32	32	16	16	16	16	16	4
9 WSS	4	16	16	16	16	16	32	32	32	32	16	16	16	16	16	4
10 WSS	4	16	16	16	16	16	32	32	32	32	16	16	16	16	16	4

Table 3.2. Constellation order per subcarrier chosen by Bit Loading technique.

Constellation Formats per SC																	
Bit & Power Loading Technique																	
	SC	1SC	2SC	3SC	4SC	5SC	6SC	7SC	8SC	9SC	10SC	11SC	12SC	13SC	14SC	15SC	16
0 WSS	16	16	16	16	16	16	16	16	16	16	16	16	16	16	16	16	16
1 WSS	16	16	16	16	16	16	16	16	16	16	16	16	16	16	16	16	16
2 WSS	8	16	16	16	16	16	16	32	32	16	16	16	16	16	16	16	8
3 WSS	8	16	16	16	16	16	16	32	32	16	16	16	16	16	16	16	8
4 WSS	8	16	16	16	16	16	16	32	32	16	16	16	16	16	16	16	8
5 WSS	4	16	16	16	16	16	32	32	32	32	16	16	16	16	16	16	4
6 WSS	4	16	16	16	16	16	32	32	32	32	16	16	16	16	16	16	4
7 WSS	4	16	16	16	16	16	32	32	32	32	16	16	16	16	16	16	4
8 WSS	4	16	16	16	16	16	32	32	32	32	16	16	16	16	16	16	4
9 WSS	4	16	16	16	16	16	32	32	32	32	16	16	16	16	16	16	4
10 WSS	4	16	16	16	16	16	32	32	32	32	16	16	16	16	16	16	4

Table 3.3. Constellation order per subcarrier chosen by Bit and Power Loading technique in a system using 16 subcarriers.

### 3.3 PCS Comparison

In this section the focus will essentially be directed to PCS and its techniques, analyzed for different scenarios as done in the previous section. The chosen parameters are the same as those considered for the Uniform QAM Constellation case, thus a number of WSS filters from 0 to 10, a number of subcarriers equal to 8, 16, 32 or 64 always compared to the single carrier case, and  $R_b$  values equal to 800G or 1.2T. For PCS a new parameter has to be taken into account: the order of the starting constellation,  $M_{PCS}$ . In Uniform QAM Constellation, in fact, to obtain 800G a constellation of 16-QAM was necessary, thus  $M = 16$ . In PCS instead the starting constellations have to be larger than the nominal one, since the shaping process reduces the overall entropy. More precisely, in this thesis, to obtain 800G the starting constellations considered are  $M_{PCS} = 64$  and  $M_{PCS} = 128$ , while for 1.2T we start from  $M_{PCS} = 128$  and  $M_{PCS} = 256$ . In figures 3.21 and 3.23 the MI values, found using a single carrier for  $\text{SNR} \in \{0..25\}$  dB and  $n\text{WSS} = 0$ , are compared in different cases to understand which of them is the most similar to the ideal one, the Shannon Limit. The Shannon Theorem, presented by Claude Shannon in 1948, refers to the maximum data rate of a communication channel that can theoretically be transferred without errors for a particular noise level. The first observable difference between the Shannon Limit and the simulations proposed is that the latter saturate at  $MI = \log_2(M)$  as the SNR increases, while, ideally, the MI should linearly increase. Instead, considering low values of SNR, the simulation curves closely follow the Shannon's one, especially in figure 3.23, where the reached MI is 6. It is interesting to notice that the lowest performance curve, in both cases, is the Uniform QAM Constellation one, suggesting that the study of PCS is actually useful for improving transmissions. In fact, the PCS curves are both above the Uniform QAM Constellation one, demonstrating even better performance when the starting constellation  $M_{PCS}$  is higher, and thus the shaping stronger. The scenario

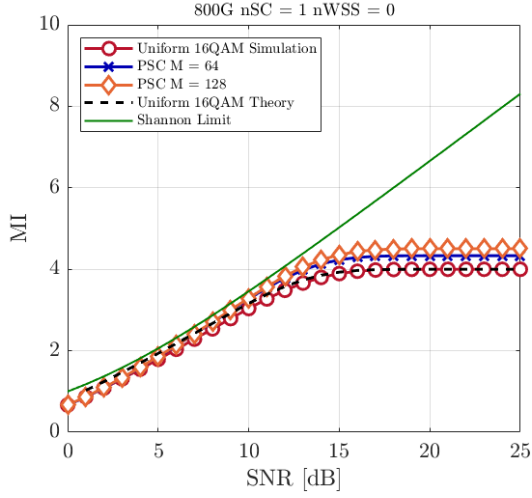


Figure 3.21. MI comparison without filters, 800 G.

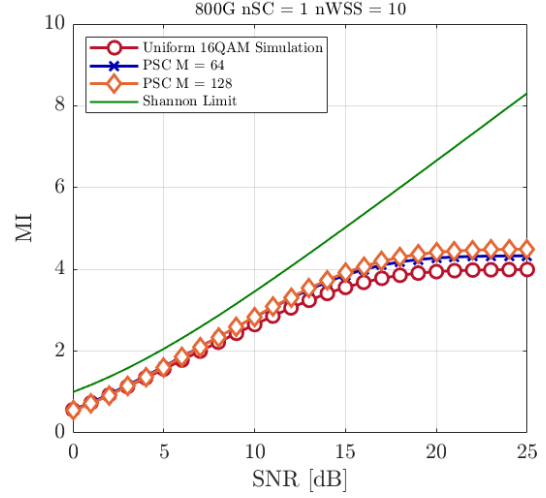


Figure 3.22. MI comparison with 10 filters, 800 G.

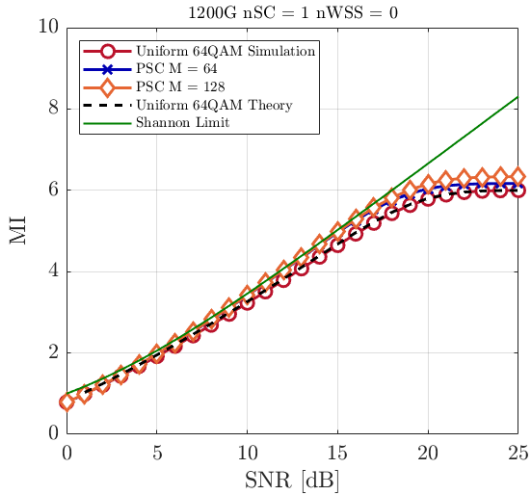


Figure 3.23. MI comparison without filters, 1.2 T.

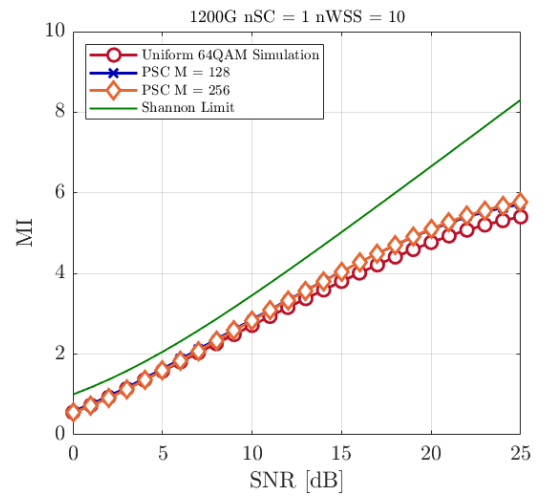


Figure 3.24. MI comparison with 10 filters, 1.2 T.

is enough changed in figures 3.22 and 3.24 where 10 filters have been inserted. Now the simulated curves are far from the Shannon's Limit for all the SNR in the range and they reach saturation for higher SNR values, in particular the ones of figure 3.24 where the saturation point is higher.

After computing the MI curves for every nWSS inserted, it is possible to find the required SNR values at the imposed target, equal to 3.33 for 800G and 5 for 1.2T. PCS performances in Single Carrier case for  $nWSS \in \{0, \dots, 10\}$  are represented in figure 3.25 for both the 800 Gbit/s and 1.2 Tbit/s cases. Here the advantage brought

by PCS is clearly evident since the corresponding Uniform QAM Constellation, the blue curve, in both plots is more than 1 dB above the other two, orange and yellow, which are the shaped ones. For the Single Carrier case, the starting constellation order  $M_{PCS}$  almost does not change the resulting  $SNR_{req}$  at all, in fact the orange and yellow curves are nearly overlapping for every nWSS.

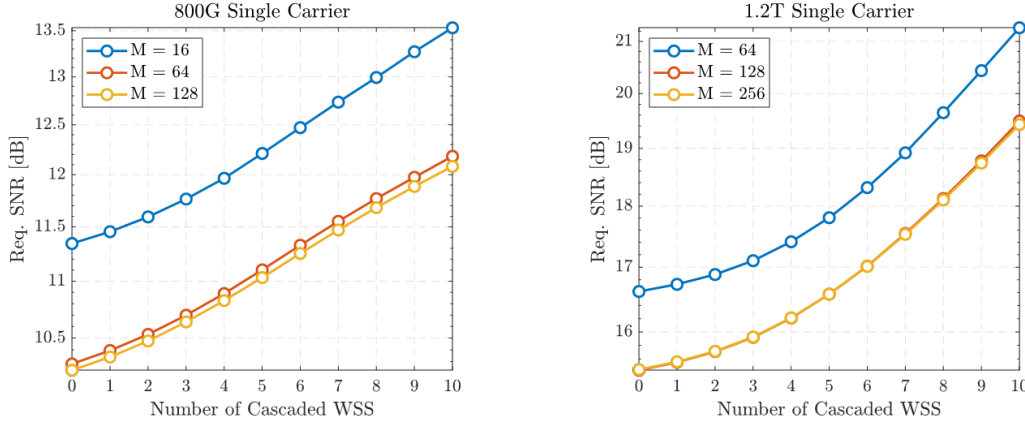
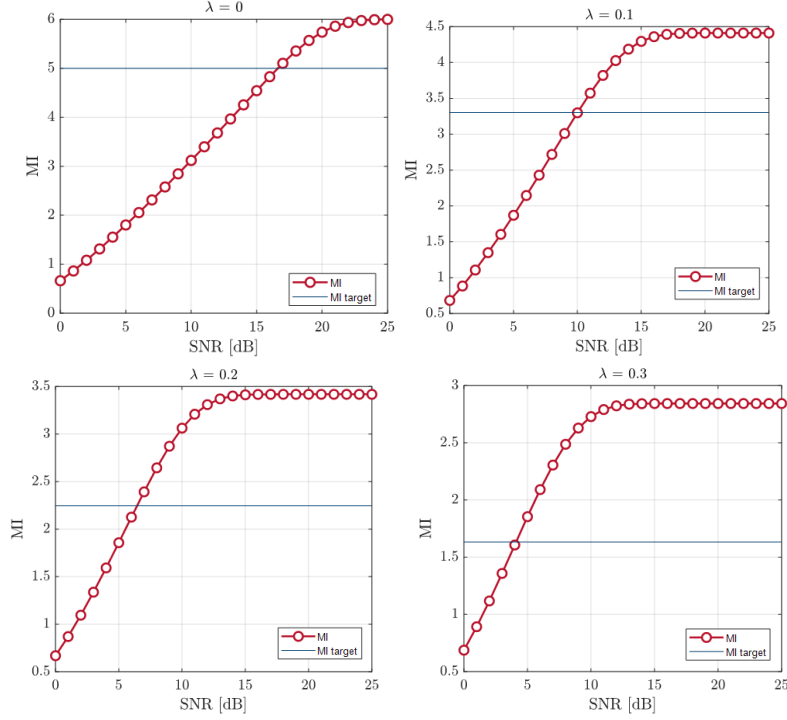


Figure 3.25. Probabilistic Constellation Shaping used in Single Carrier systems.

In all the above mentioned graphs the PCS is considered just exploiting the Same Power technique, so the improvements with respect to the uniform constellation are only brought by the shaping of the probability distribution function.

As previously mentioned,  $\lambda$  is a fundamental PCS parameter since it defines how much the Maxwell-Boltzmann distribution, whose expression is reported in Eq. 2.17, is shaped. The higher its value, the higher the probability of central symbols and the lower the probability of external symbols. On the contrary, a  $\lambda$  value equal to 0 will keep the probability of occurrence uniform over all the constellation points. As  $\lambda$  varies, the channel bit rate changes and, consequently, so does MI, target MI, and target SNR. Table 3.3 for example shows the  $R_b$  values obtained by varying  $\lambda$  between 0 and 0.5 for a constellation  $M_{PCS} = 64$ ; when  $\lambda = 0$   $R_b$  is the maximum obtainable since this case coincides with Uniform QAM Constellation, i.e.  $R_b = 1.2$  Tbit/s. Instead, when  $\lambda$  increases the bit rate will decrease, a consequence of the fact that the constellation will have less probable symbols to use. Table 3.3 shows also the variation of MI target, since it is computed starting from the Bit Rate, if  $R_b$  decreases also MI target will decrease. Some MI curves are reported in figure 3.26 for different imposed  $\lambda$  values, as anticipated, just the first one with  $\lambda = 0$  is able to reach  $\log_2(64) = 6$  bits/symbol. A more comprehensive MI trend can be found in the 3-D plot of figure 3.27, from which it can be retrieved that the MI depends on both SNR and  $\lambda$ . This gives the hint that the calculation of the  $\lambda$  value allowing the system to reach the target MI depends on the considered value of SNR; that is a fundamental concept for the development of Entropy Loading, where, before

$\lambda$	0	0.05	0.10	0.15	0.20	0.25	0.30	0.35	0.40	0.45	0.50
$R_b$ Gbit/s	1200	1014.1	793.1	644.7	538.6	456.8	391.6	339.6	298.6	266.8	242.6
MI target	5.0	4.22	3.30	2.68	2.24	1.90	1.63	1.41	1.24	1.11	1.01

 Table 3.4.  $R_b$  and  $MI_{target}$  values for different  $\lambda$ .

 Figure 3.26. MI and  $MI_{target}$  variation with respect to  $\lambda$ .

simulating, the suitable  $\lambda$  vector (of length  $1 \times n_{SC}$ ) has to be calculated for each SNR value.

As it has already been stated, the required SNR value depends on  $\lambda$  with a trend reported in figure 3.28; if  $\lambda$  increases,  $SNR_{req}$  decreases, meaning that the more the constellation is shaped, the lower the required SNR is. This makes sense because a shaped constellation is smaller than the respective nominal one, so it requires a lower SNR to be reliable. In the figures it is shown also how the number of cascaded WSS changes the performances in both the Single Carrier and the 8 subcarriers cases. It can be found that, if  $n_{WSS} = 0$  produces the same curve in both types, as the  $n_{WSS}$  becomes more consistent the effects result to be more evident with 8 subcarriers. The colored curves are indeed more separated in the right graph with respect to the other, meaning that filtering effects have more impact if the number of subcarriers is higher, while the single case one remains the most robust

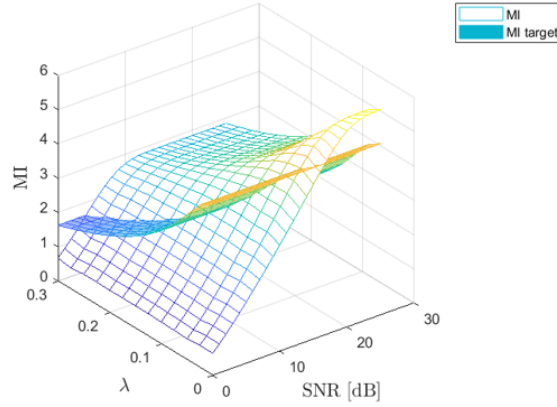


Figure 3.27. 3-D plot showing how the MI value depends on both SNR and  $\lambda$ .

against channel impairments. Since  $\lambda$  is inversely proportional to  $R_b$ , as shown in

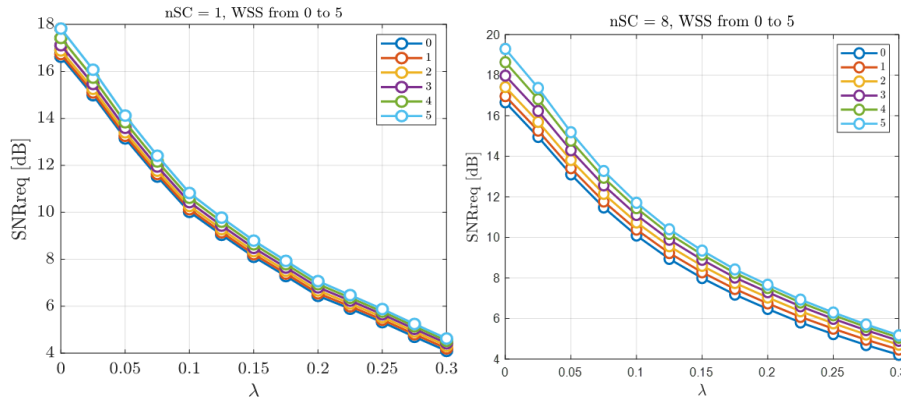


Figure 3.28. Required SNR vs  $\lambda$  with  $nWSS \in \{0..5\}$ , for both Single Carrier and 8 subcarriers cases.

Table 3.3, if  $SNR_{req}$  increases with  $\lambda$ , it decreases with  $R_b$ . Figure 3.29 illustrates the relation between  $SNR_{req}$  and  $R_b$ . It can be noticed that  $R_b$  ranges from less than 400 G to 1.2 T that, referring to table 3.3, exactly correspond to the  $\lambda$  range  $\{0..0.3\}$ . In fact, it has been already stated that 1.2 T is achieved for  $M_{PCS} = 64$  no shaped, thus  $\lambda = 0$ . Also in this plots it is clear that the filtering effect has more impact with 8 subcarriers than with just a single carrier. Widening the range of  $\lambda$  values up to 0.5, like in table 3.3, the reachable  $R_b$  values would be lower than 400 G, so the left side of graphs in figure 3.29 would be expanded.

Let's now focus on Entropy Loading (EL), which, as already stated, it consists in the optimization of the shaping factor  $\lambda$  for each subcarrier.

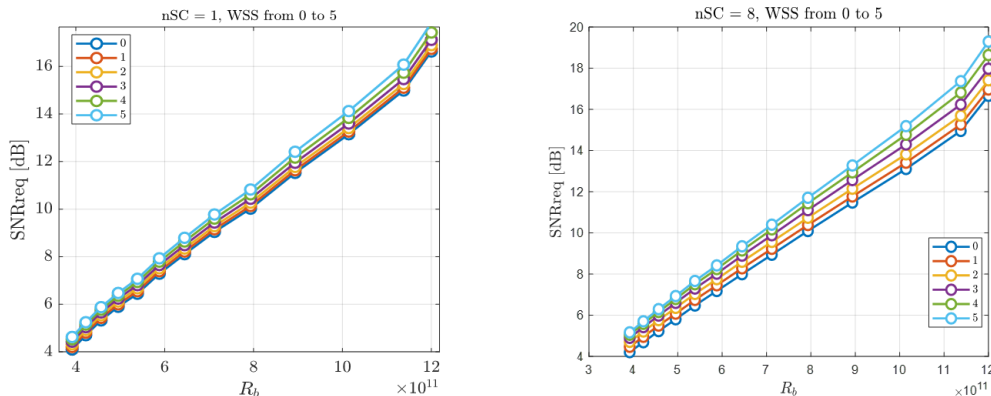


Figure 3.29. Required SNR vs  $R_b$  with  $nWSS \in \{0..5\}$ , for both Single Carrier and 8 subcarriers cases.

As was already done in the investigations carried out in case of uniform modulation, the EL analysis starts with the study of the theoretical predictions of both MI and  $SNR_{req}$ . In figure 3.30 are compared the simulated MI with the theoretical one found applying EL in 4 different cases. In the first two images, where the bit rate is set to 800G, the 8 subcarriers system switches from 0 to 10 filters and the two curves that were initially overlapped become completely separated. On the contrary, the latter images, for the 1.2T system, show that with an higher number of subcarriers, 32 in this case, the simulation remains close to the theory, meaning that with several subcarriers the theoretical prediction is more accurate. The reason for this improvement, as was already discussed in the previous section, is related to the better approximation of the WSS filter transfer function. This behavior is unequivocally evident in figures 3.31, in which the two curves, as nSC increases, become closer until they overlap. In the top-left graph the curves appear to be far apart, they are actually separated by slightly more than 1 dB at most. The lower figures, with  $nSC = 32$  and  $nSC = 64$ , are those in which simulation and theory results are almost the same. The relevant difference in first image, instead, is a consequence of a combination of reasons. First of all, theory is, as usual, an optimistic prediction of simulation since it does not provide an accurate estimation of the impact of filtering effects on the edge subcarriers when the number of subcarriers is not large enough, as already discussed previously. Moreover, since the  $\lambda$  optimization step in the EL algorithm is based on theory, and it has been stated that theory is not an exact prediction, then those  $\lambda$  values are not actually the optimal, so the  $SNR_{req}$  values from simulation are higher than expected, making the gap between the two curves even larger.

A key concept of the EL algorithm is that, after setting nWSS, the optimal  $\lambda$  vector ( $1 \times nSC$ ) is retrieved for every SNR value belonging to a given range. This means that to each SNR value is associated a  $\lambda_{opt}$  vector. Then, in the time-domain

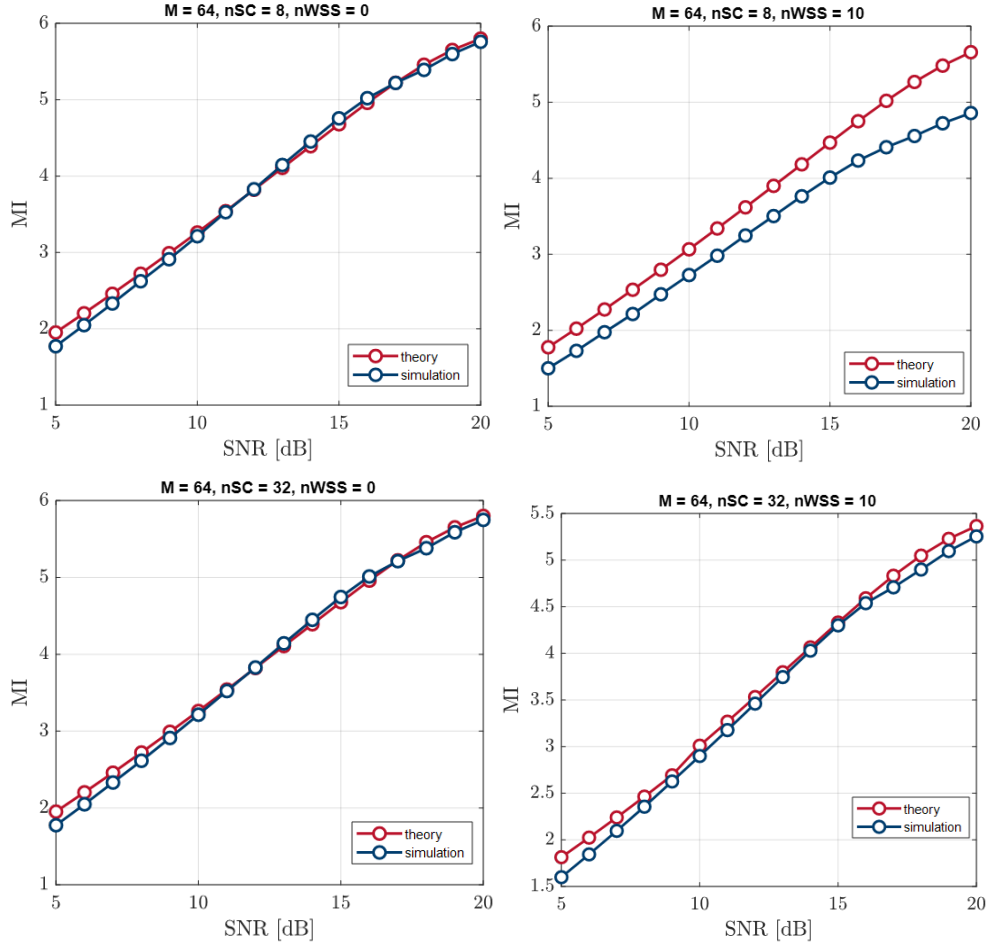


Figure 3.30. Comparison of MI values obtained through theory and simulation in different conditions.

simulation, each SNR value under test is associated to its optimum lambda vector,  $\lambda_{opt}$ , that guarantees the best performances in term of MI and  $SNR_{req}$ .

To better explain the concept, each point from the graphs of figure 3.30 is obtained for a certain level of SNR of the system (from 5 dB to 20 dB) transmitting a constellation shaped with a lambda vector (of length 1x8) optimal for that SNR value. In figure 3.32, by contrast, each lambda vector is used for the entire range of SNR, so each point in the previous graph is expanded into a different colored curve. The black line corresponds to the blue line of the second graph in fig 3.30, and is constructed exploiting the optimal lambda values, in fact it stands above all others. Another proof to show that the use of  $\lambda_{opt}$  is the best in terms of performances was done by selecting the  $\lambda_{20dB}$  orange curve and cut it at the  $MI_{target}$ . The so obtained  $SNR_{req}$  is 12.75 dB, which is greater than the one achieved exploiting  $\lambda_{opt}$ , which is  $SNR_{req} = 12.33$  dB.

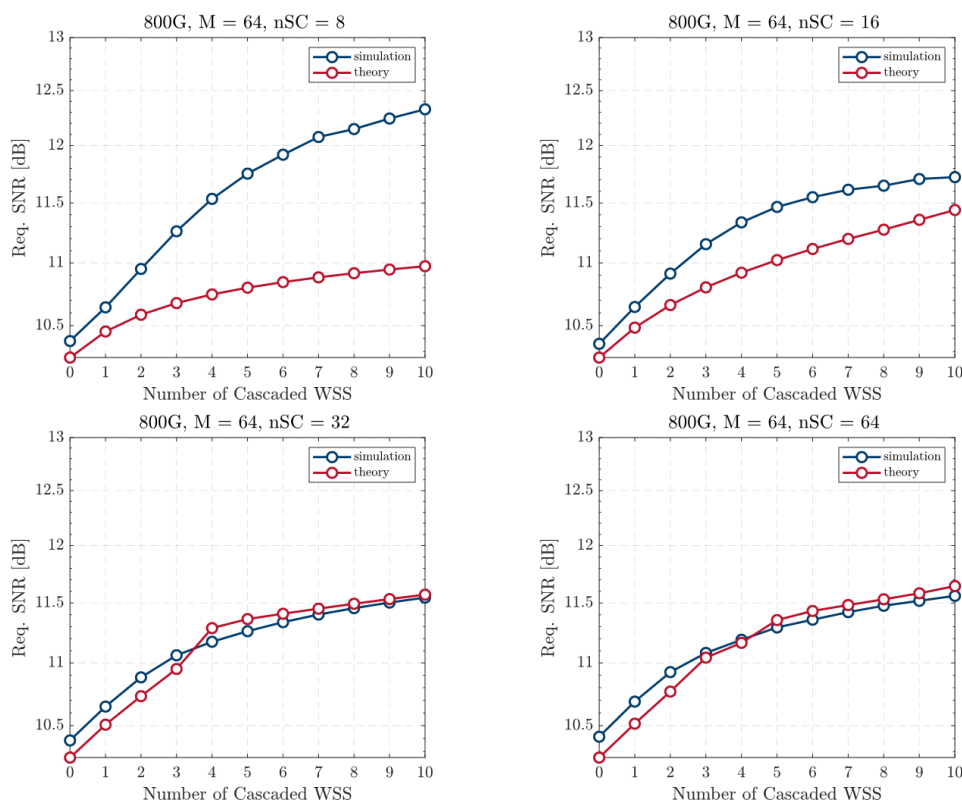


Figure 3.31. Comparison between theory and time-domain simulation for Entropy Loading with  $nSC = 8, 16, 32, 64$ .

Table 3.5 reports the  $\lambda$  values related to the required SNRs found after the optimization for the following parameters:  $nSC=8$ ,  $M=64$ ,  $800G$ . These  $\lambda$ s are not the ones directly tested, but instead they have been retrieved going backwards from the obtained  $SNR_{req}$ , making an interpolation with the  $\lambda_{opt}$  associated to each SNR value. As expected, without filters each subcarrier has the same  $\lambda$ , so the shaping is the same for every subcarrier's constellation; increasing the number of filters instead, the outer subcarriers result to be more shaped than the inner ones.

In Chapter 2 it was already introduced that Entropy Loading technique can be applied with or without a power optimization strategy called Water Filling which aims to redistribute power by penalizing the most impaired subcarriers. To understand how Water Filling acts in practice, some Power Ratio values have been reported in table 3.6. The considered system is composed by 8 subcarriers, 10 WSS filters and  $M_{PCS} = 64$ , five SNR values have been tested to show that the initial Signal-to-Noise ratio influences the power redistribution. All the ratios are in dB and, according to the mentioned graphical representation, lower values are assigned to the outer subcarriers. It's interesting to compare this table to the one reporting the values found from Power Loading technique (figure 3.1), because they behave

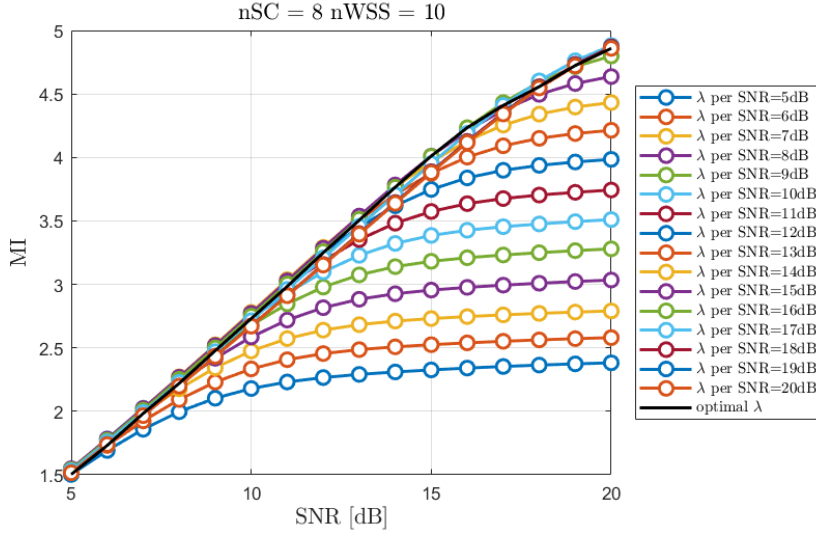


Figure 3.32. MI versus SNR obtained for vectors of shaping factors optimized for different levels of SNR.

$\lambda$ per SC								
Entropy Loading and Water Filling Technique								
nWSS	SC 1	SC 2	SC 3	SC 4	SC 5	SC 6	SC 7	SC 8
0	0.1291	0.1291	0.1291	0.1291	0.1291	0.1291	0.1291	0.1291
1	0.1466	0.1215	0.1215	0.1215	0.1215	0.1215	0.1215	0.1466
2	0.1546	0.1131	0.1131	0.1131	0.1131	0.1131	0.1131	0.1546
3	0.1578	0.1057	0.1057	0.1057	0.1057	0.1057	0.1057	0.1578
4	0.1589	0.0996	0.0996	0.0996	0.0996	0.0996	0.0996	0.1589
5	0.1592	0.0947	0.0947	0.0947	0.0947	0.0947	0.0947	0.1592
6	0.1599	0.0908	0.0908	0.0908	0.0908	0.0908	0.0908	0.1599
7	0.1601	0.0876	0.0876	0.0876	0.0876	0.0876	0.0876	0.1601
8	0.1626	0.0862	0.0862	0.0862	0.0862	0.0862	0.0862	0.1626
9	0.1641	0.0844	0.0844	0.0844	0.0844	0.0844	0.0844	0.1641
10	0.1653	0.0827	0.0827	0.0827	0.0827	0.0827	0.0827	0.1653

Table 3.5. Shaping factor  $\lambda$  optimized for all subcarriers for different number of cascaded WSS using EL and WF techniques.

completely in the opposite way. In fact, PL assigns more power if the subcarrier suffers from filtering in order to mitigate the impairments, the drawback is the possible power wasting in subcarriers too much corrupted to transmit a reliable signal. The negative ratios, indeed, can be found in table 3.6 only for SC 1 and 8, while in table 3.1 every ratio is a negative number, except SC 1 and 8. Another possible observation is that an higher SNR reduces the PR gap between subcarriers, in other words, the PR increases in the outer SCs while it decreases in the inner ones, confirming that a stronger input signal enhances the performances of the system. To show the effective improvements brought by the combined usage of Water Filling and Entropy Loading, graphs are reported in figure 3.33; despite they are limited

Power Ratios per SC								
Entropy Loading and Water Filling Technique $nWSS = 10$								
SNR	SC 1	SC 2	SC 3	SC 4	SC 5	SC 6	SC 7	SC 8
5 dB	-1.1288	0.3193	0.3193	0.3193	0.3193	0.3193	0.3193	-1.1288
6 dB	-0.8715	0.2555	0.2556	0.2556	0.2556	0.2556	0.2555	-0.8715
7 dB	-0.6774	0.2042	0.2042	0.2042	0.2042	0.2042	0.2042	-0.6774
8 dB	-0.5292	0.1629	0.1630	0.1630	0.1630	0.1630	0.1629	-0.5292
9 dB	-0.4149	0.1299	0.1300	0.1300	0.1300	0.1300	0.1299	-0.4149

Table 3.6. Power Ratio for different SNR values using Waterfilling technique.

to the usual case of 800G and  $M_{PCS} = 64$ , a general behaviour can be retrieved. The first impression is that the WF effect is slightly improves the overall systems performance, in fact, with WF the required SNRs turn out to be just a little lower than those found without WF in all the graphs. More precisely, with  $nSC = 8$  the blue and red curves approximately coincide, while with an higher subcarriers number they split as the number of WSS increases. However, the gap between the two curves is limited to 0.5 dB, even in the case of the last graph with  $nSC = 64$ , which apparently is where WF is able to have the largest impact. These considerations are not intended to discredit the effectiveness of such a well-known technique as Water Filling, but rather to emphasize the great performance already achieved by Entropy Loading, whose further optimization may be considered not that essential. However, since the Water Filling application has a very low computational cost, Entropy Loading will always be combined with Water Filling in the following analyses in order to obtain the best possible result.

In this last part on PCS, the several discussed strategies will be compared, exactly as it was previously done for the Uniform QAM Constellation. For the 800G bit rate case two different  $M_{PCS}$  have been taken into account:  $M_{PCS} = 64$  and  $M_{PCS} = 128$ ; obviously also higher values could be used, but these two are sufficient to understand the advantage of the shaping technique. The plots of figure 3.34 are differentiated by the number of subcarriers that, as already done before, goes from 8 to 64. In all the four graphs is reported as reference the Single Carrier curve obtained using PS over a  $M_{PCS}=128$  constellation, this curve was chosen for being the lowest one in the left graph of figure 3.25, so it is the case in which just PS is used, not MSC. Therefore, the following comparisons highlight the advantages of using a multi-subcarriers system over the single carrier one when considering PCS modulation. The other four curves, in each plot, are divided into: two curves of Probabilistic Shaping with Same Power technique (PCS  $M = 64 + SP$ , PCS  $M = 128 + SP$ ), so each subcarrier will have the same  $\lambda$  value and power, and the other two with Entropy Loading and Waterfilling (PCS  $M = 64 EL \& WF$ , PCS  $M = 128 EL \& WF$ ), meaning that each subcarrier has an optimal  $\lambda$  value depending on the attenuation of the filters. The first thing to notice is that in the first graph, corresponding to  $nSC = 8$ , no curve can get under the Single Carrier one, stating that in this conditions the MSC approach does not bring any advantages. So it

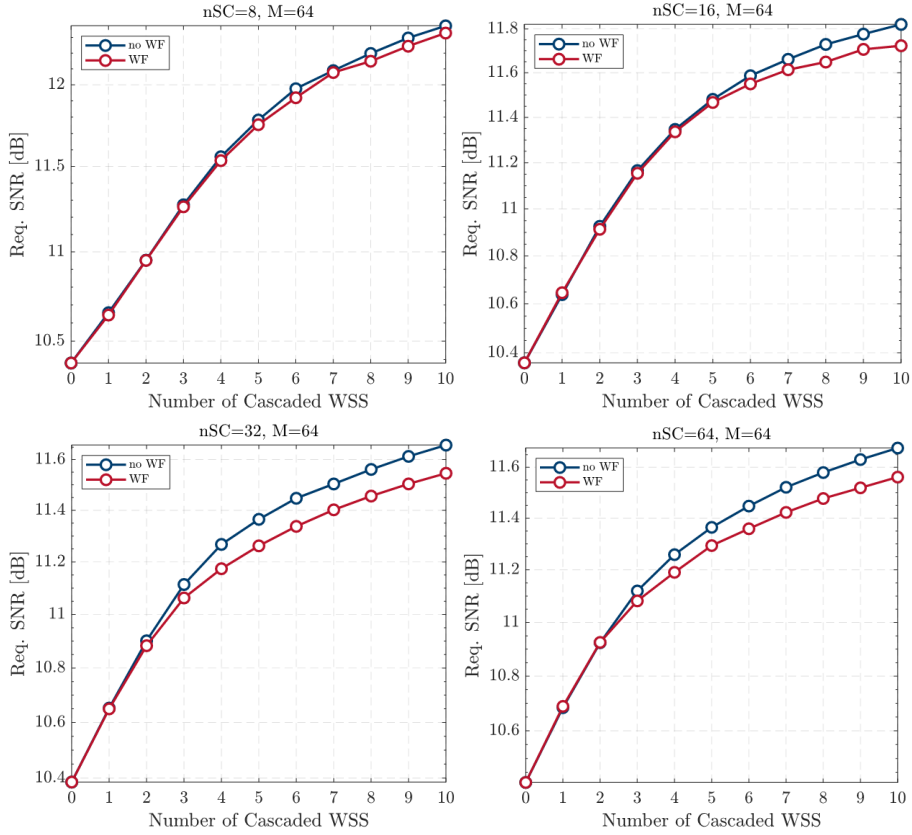


Figure 3.33. Comparison between Entropy Loading with and without Waterfilling in the 800G system for different number of subcarriers.

can be concluded that, just as with Uniform QAM Constellation, the worst case is obtained using 8 subcarriers also with PCS. Increasing the number of subcarriers things get better for PS and EL, in fact, their curves are able to cross the single carrier one for a sufficiently high number of nWSS. However, the same trend is evident in all the four graphs and we can conclude that an higher initial constellation order  $M_{PCS}$  reaches higher performances and that Entropy Loading performs better than Same Power. This means that the order of the curves, from the top to the bottom, is the same despite the different nSC imposed.

The 1.2T case has been reported using the same format in figure 3.35. In this case the chosen  $M_{PCS}$  are 128 and 256, and the respective four curves are compared with the Single Carrier  $M_{PCS} = 256$ , already illustrated in the second graph of figure 3.25. These graphs confirm what was earlier said on the order of the curves, thus the best combination is made applying Entropy Loading and Waterfilling on a  $M_{PCS} = 256$  constellation. PS and EL seem to perform generally better in this last 1.2T case, in fact, the colored curves are able to cross the black one at a lower

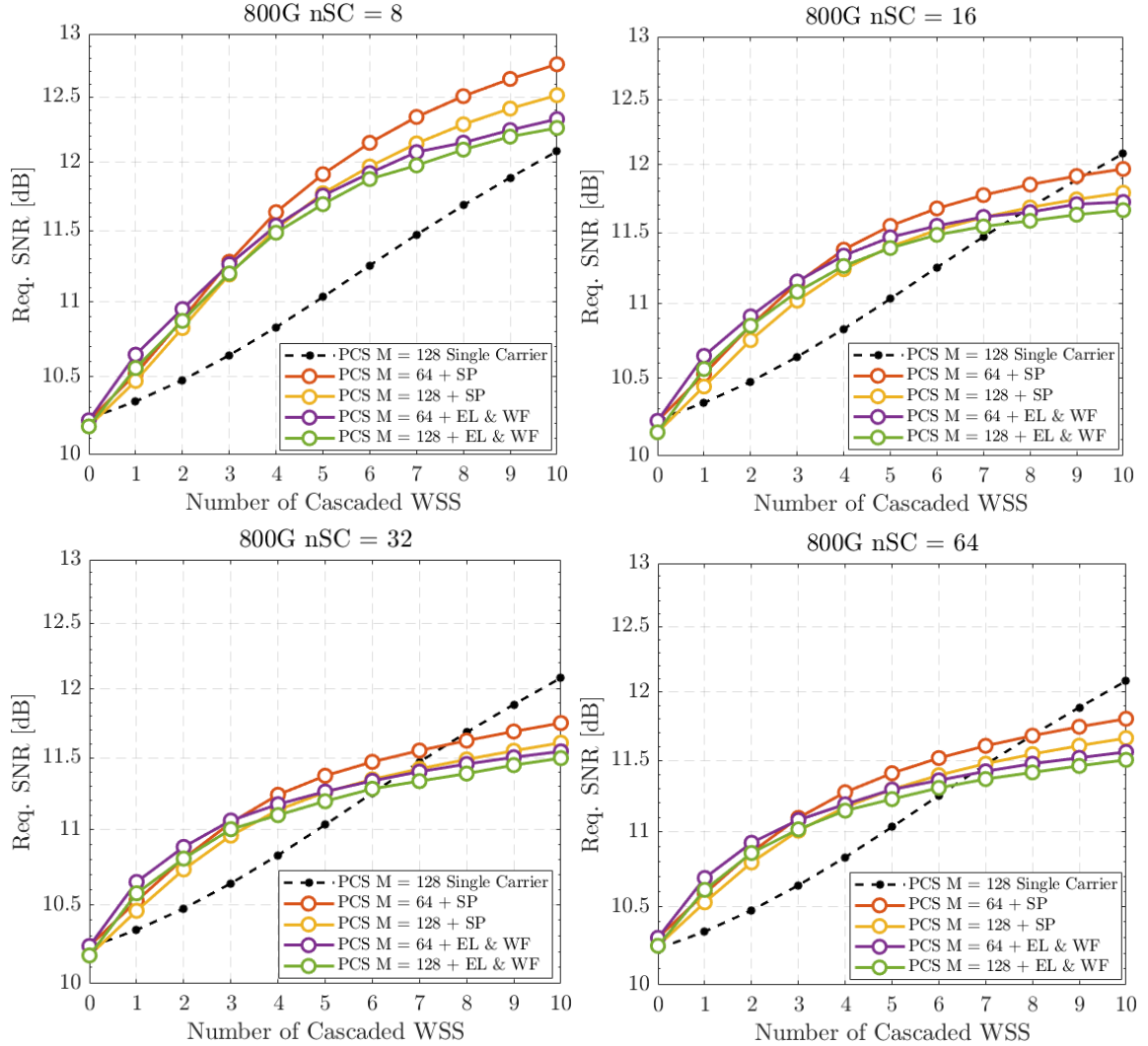


Figure 3.34. 800G PCS applied with nSC = 8, 16, 32, 64. PCS + SP stands for PCS using the Same Power strategy, PCS + EL & WF for PCS using both the Entropy Loading and Waterfilling strategies.

number of filters than before, also in the nSC = 8 case.

The last comparison for this section, in figure 3.36, is made just among Entropy Loading results, fixing the bit-rate and the initial constellation order while changing the number of subcarriers. In addition, for each bit-rate, only the highest  $M_{PCS}$  between the two previously considered has been chosen, so  $M_{PCS} = 128$  for 800G and  $M_{PCS} = 256$  for 1.2T. These limitations have been introduced in order to compare just the curves achieving the best performances in the figures 3.34 and 3.35. As expected, the 8 subcarriers configuration needs the highest  $SNR_{req}$  values in both scenarios, confirming to not be the right choice for this type of transmission. On

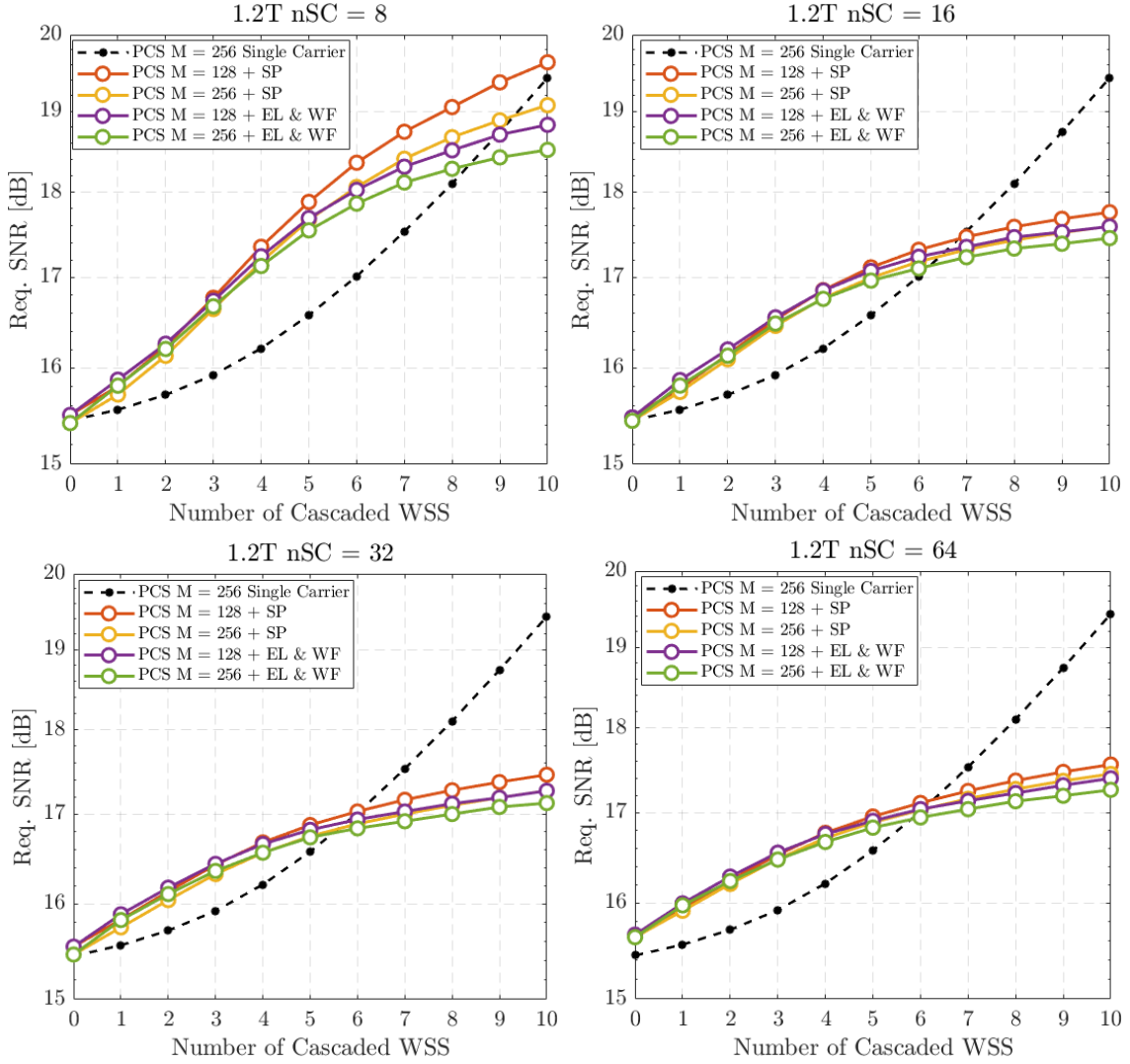


Figure 3.35. 1.2T PCS applied with  $nSC = 8, 16, 32, 64$ . PCS + SP stands for PCS using the Same Power strategy, PCS + EL & WF for PCS using both the Entropy Loading and Waterfilling strategies.

the other hand, the best performance is reached by 32 subcarriers, its advantage is barely noticeable with 800G where the 32 SC curve is almost completely overlapped by 64 SC but quite clear for 1.2T. To conclude, in both graphs the curves apparently keep the same trend, but it has to be noticed that the second one is referred to higher  $SNR_{req}$  values, in fact, there is about a 5 dB gap between the two.

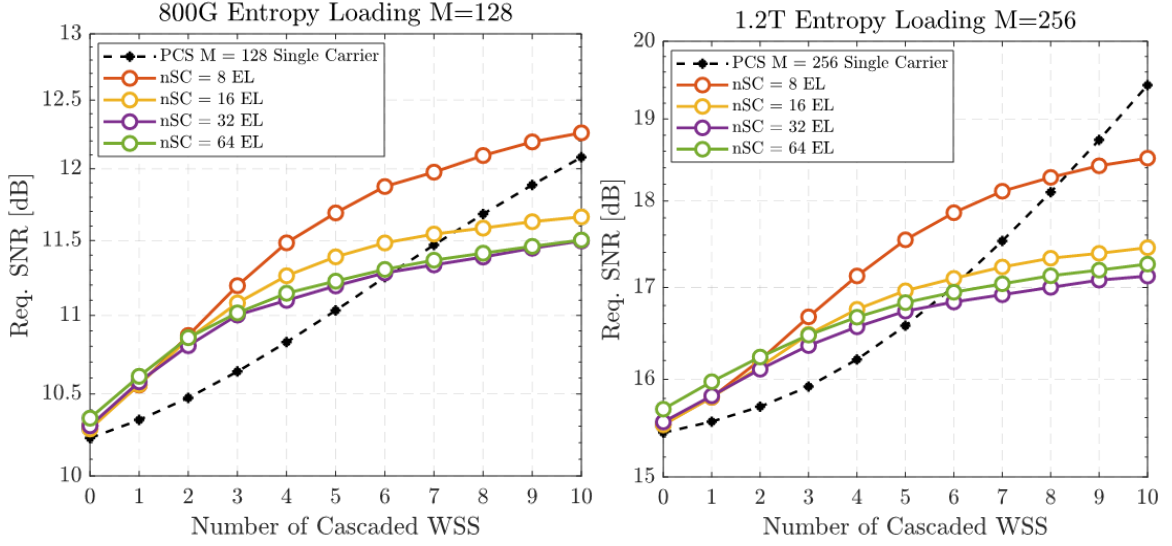


Figure 3.36. 800G and 1.2T Entropy Loading for different nSC.

### 3.4 Uniform QAM Constellation and PCS Comparison

This last section compares separately the two modulation families discussed so far, Uniform QAM Constellation and Probabilistic Constellation Shaping. It has already been explained in section 3.1 that in order to compare the two modulations, the simulation results must have been obtained using the same metric, otherwise they would be not comparable, as in the example shown in figure 3.3. In the previous analysis, Uniform QAM Constellation was studied considering the BER as performance metric, while PCS performance analysis was based on MI, because BER, which is based on counting received erroneous bits, cannot be used with PCS. It follows that, in order to compare the two modulations, MI is the only possible option. To be able to do this, the  $SNR_{req}$  of some Uniform QAM Constellation simulations were re-obtained by cutting the calculated MI curve at the MI target, instead of using BER, for each number of filters. Nevertheless, at this point not all Uniform QAM Constellation strategies have been taken into consideration; in fact, together with the Same Power technique, only Bit Loading was chosen, since in the previous analysis it proved to be the most advantageous. On the contrary, Power Loading was excluded as it turned out to be quite inefficient in all tested cases while Bit & Power Loading is too slow to be applied in all conditions and does not bring significant improvement over Bit Loading.

Figure 3.37 shows all graphs referring to a total bit rate of 800 Gbit/s splitting them according to the number of subcarriers nSC. In each graph there are

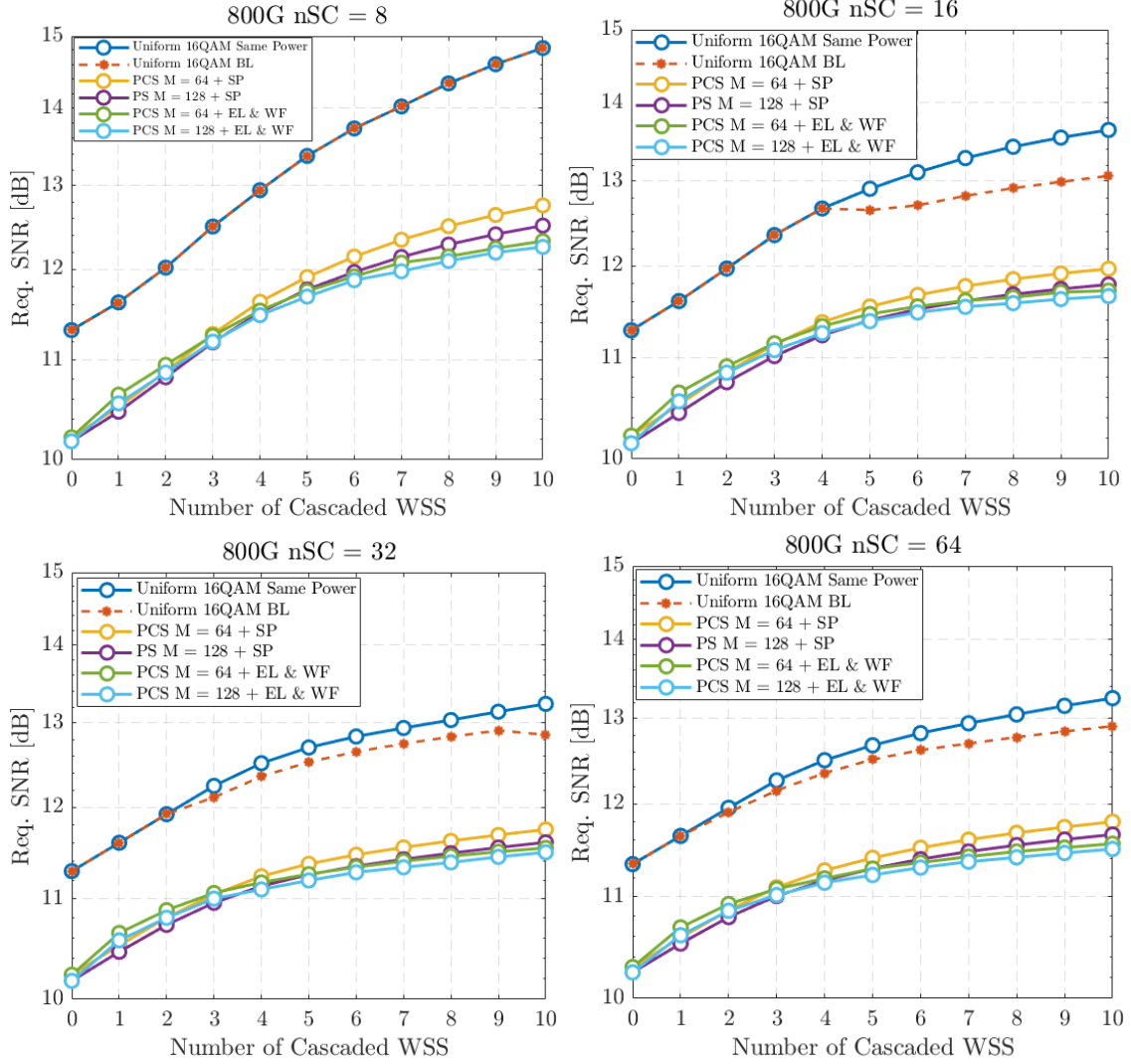


Figure 3.37. Uniform QAM Constellation and PCS final comparison for 800G.

two Uniform QAM Constellation curves, Same Power and Bit Loading, and four Probabilistic Constellation Shaped curves, two using just PS and two with Entropy Loading and Waterfilling. The same comparison was repeated in figure 3.38 for 1.2Tbit/s total bit rate.

Analyzing the Uniform QAM Constellation results through MI, BL does not seem to have the same impact as in the previous comparison, obtained from BER. In fact, it allows to gain just about 0.2 dB with respect to the Same Power technique. On the other hand, PCS proves to be the best among MSC approaches already using the simple Probabilistic Shaping, the combination of techniques such as EL and WF do not particularly lower the SNRreq.

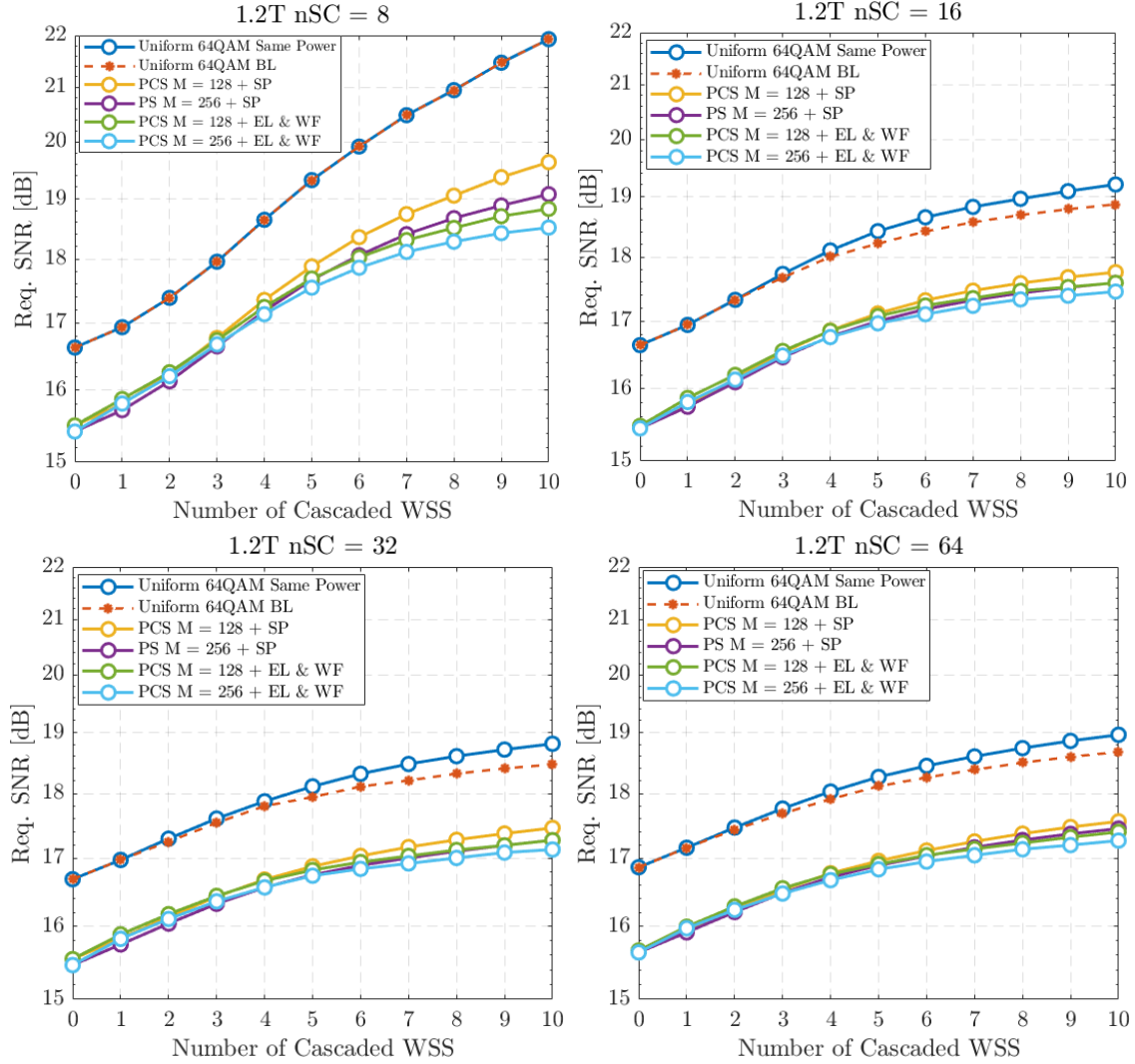


Figure 3.38. Uniform QAM Constellation and PCS final comparison for 1.2T.

In all the above figures there isn't any Single Carrier curve to use as a reference, because Uniform QAM Constellation and PCS cannot be compared with the same SC curve, in fact in their respective sections, Uniform QAM Constellation referred to a Uniform 16 or 64 QAM constellation Single Carrier, while PCS to a Shaped  $M_{PCS} = 128$  or  $M_{PCS} = 256$  constellation Single Carrier. For completeness of information, the Single Carrier curves are reported in figure 3.39 and the gap between them proves that the PCS is more advantageous than Uniform QAM Constellation even without the use of MSC.

These graphs in figure ??, in conclusion, show that there is a substantial difference between the results of the two modulation techniques, PCS is able to almost always

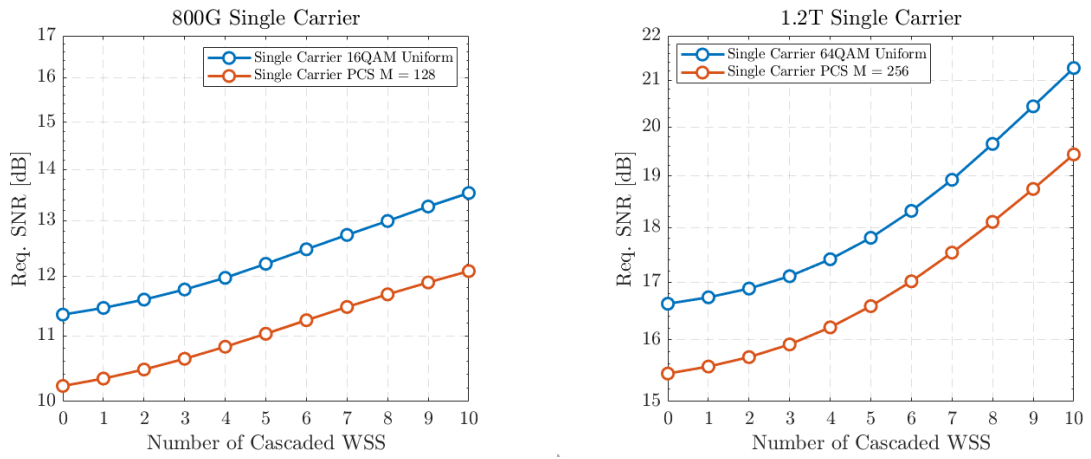


Figure 3.39. Single Carrier comparison for 800G and 1.2T.

achieve more than 1 dB of advantage with respect to Uniform QAM Constellation's Bit Loading.

# Chapter 4

## Conclusions

The goal of this thesis is to study and compare different transmission techniques based on the multi-subcarrier approach (MSC) for optical communication systems. This approach is relevant due to its ability to mitigate the ROADMs filtering effect, which degrades edge frequencies. In this work the studied transmission systems are 800 Gbit/s and 1.2 Tbit/s both operating at 128 GBaud symbol rate. The signal, instead, has been tested using different modulation formats and optimization strategies in order to understand which combination can better reduce the impact of ROADMs. The MSC approach has been tested for different number of subcarriers, in particular  $n_{SC} = 8, 16, 32, 64$ . In the presented simulations, the number of inserted filters ranges from 0 to 10, an appropriate number that corresponds to have up to 5 ROADMs along the lightpath from source to destination.

The studied modulation techniques are divided into two main groups, Uniform QAM Constellation and Probabilistic Constellation Shaping. The strategy, among the Uniform QAM Constellation ones, that emerges as the most prominent is Bit Loading, because it turns out to be an acceptable compromise between benefits and computational costs. However, the most important topic of the thesis is the application of PCS, a newer and more complex approach to signal modulation. The use of PCS on a Single Carrier signal is already able to significantly improve the performances of the system compared to the Uniform QAM Constellation case. However, the MSC approach performs better when the number of WSS becomes high, in fact under these conditions, the SNR required by the PCS system to guarantee a certain BER or MI threshold is lower than using a Uniform QAM Constellation.

It has also been shown that the theoretical performance prediction is not recommended for the 8 and 16 subcarriers systems, since the results tend to be too optimistic with respect to the real simulation. On the other hand, it performs quite well with 32 and 64 subcarriers, in which it could be used to correctly predict the simulation results.

The newer PCS technique presented in this work is Entropy Loading, which succeeds for both 800G and 1.2T in further lowering the  $SNR_{req}$ . Its advantage,

however, results less efficient when the PCS initial constellation  $M_{PCS}$  is large, for example 128-QAM with 800G or 256-QAM at 1.2T, because a large constellation already gains in dB. The other technique that can be used combined with EL, the Waterfilling, achieves slight improvements optimizing the power distribution among the subcarriers, even if its effect is not so decisive, it has been concluded to apply it anyway given its small cost in terms of computational time.

What is clear from all the tested cases is that the best MSC configurations are those with 32 and 64 subcarriers, corresponding to 32 x 4 GBaud and 64 x 2 GBaud signals.

# Bibliography

- [1] F.P. Guiomar, L. Bertignono, A. Nespola, A. Carena, in “Frequency-Domain Hybrid Modulation Formats for High Bit-Rate Flexibility and Nonlinear Robustness”, *Journal of Lightwave Technology*, Vol. 36, N. 20, (October 2018).
- [2] Meng Qiu, Qunbi Zhuge, Mathieu Chagnon, Yuliang Gao, Xian Xu, Mohamed Morsy-Osman, and David V. Plant in "Digital subcarrier multiplexing for fiber nonlinearity mitigation in coherent optical communication systems".
- [3] Y. Li, J. Li, L. Zong, S. K. Bose and G. Shen, in “Upgrading Nodes with Colorless, Directionless, and/or Contentionless ROADMs in an Optical Transport Network”, *2020 22nd International Conference on Transparent Optical Networks (ICTON)*, 2020, pp. 1-4.
- [4] C. Pulikkaseril, L. A. Stewart, M. A. F. Roelens, G. W. Baxter, S. Poole, and S. Frisken, in “Spectral modeling of channel band shapes in wavelength selective switches”, *Opt. Express* 19(9), 8458–8470 (2011).
- [5] A. M. Rosa Brusin., P. Guiomar, A. Lorences-Riesgo, P.P. Monteiro and A. Carena in "Enhanced resilience towards ROADM-induced optical filtering using subcarrier multiplexing and optimized bit and power loading", *Opt. Express* 30710, Vol. 27, No. 21 / 14 October 2019.
- [6] F.P. Guiomar et al., "Adaptive Probabilistic Shaped Modulation for High-Capacity Free-Space Optical Links", *Journal of Lightwave Technology*, vol. 38, no. 23, pp. 6529-6541, 1 Dec.1, 2020, doi: 10.1109/JLT.2020.3012737.
- [7] D. Che and W. Shieh, "Approaching the Capacity of Colored-SNR Optical Channels by Multicarrier Entropy Loading", *Journal of Lightwave Technology*, vol. 36, no. 1, pp. 68-78, 1 Jan.1, 2018, doi: 10.1109/JLT.2017.2778290.
- [8] T. Rahman et al., “On the mitigation of optical filtering penalties originating from ROADM cascade,” *IEEE Photon. Technol. Lett.*, vol. 26, no. 2, pp. 154–157, Jan. 2014.
- [9] D. Che and W. Shieh, "Squeezing out the last few bits from band-limited channels with entropy loading, *Opt. Express* 27, 9321-9329 (2019).
- [10] M. Qiu et al., “Digital subcarrier multiplexing for fiber nonlinearity mitigation in coherent optical communication systems,” *Opt. Express*, vol. 22, no. 15, pp. 18770–18777, Jul. 2014.

- [11] F.P. Guiomar, A. Carena, G. Bosco, L. Bertignono, A. Nespola, and P. Poggiolini, "Nonlinear mitigation on subcarrier-multiplexed PM16QAM optical systems," *Opt. Express*, vol. 25, no. 4, pp. 4298–4311, Feb. 2017.
- [12] [https://phabrix.com/ftp/App\\_Notes/Stress\\_Whitepaper.pdf](https://phabrix.com/ftp/App_Notes/Stress_Whitepaper.pdf)
- [13] <https://www.ni.com/it-it/innovations/white-papers/06/pulse-shape-filtering-in-communications-systems.html>